

Metamorphism of Greater and Lesser Himalayan rocks exposed in the Modi Khola valley, central Nepal

Aaron J. Martin · Jibamitra Ganguly ·
Peter G. DeCelles

Received: 4 March 2009 / Accepted: 8 July 2009 / Published online: 4 August 2009
© Springer-Verlag 2009

Abstract Thermobarometric estimates for Lesser and Greater Himalayan rocks combined with detailed structural mapping in the Modi Khola valley of central Nepal reveal that large displacement thrust-sense and normal-sense faults and ductile shear zones mostly control the spatial pattern of exposed metamorphic rocks. Individual shear zone- or fault-bounded domains contain rocks that record approximately the same peak metamorphic conditions and structurally higher thrust sheets carry higher grade rocks. This spatial pattern results from the kinematics of thrust-sense faults and shear zones, which usually place deeper, higher grade rocks on shallower, lower grade rocks. Lesser Himalayan rocks in the hanging wall of the Ramgarh thrust equilibrated at about 9 kbar and 580°C. There is a large increase in recorded pressures and temperatures across the Main Central thrust. Data presented here suggest the presence of a previously unrecognized normal fault entirely within Greater Himalayan strata, juxtaposing hanging wall rocks that equilibrated at about 11 kbar and 720°C against footwall rocks that equilibrated at about 15 kbar and 720°C. Normal faults occur at the structural top and within the Greater Himalayan series, as well as in Lesser

Himalayan strata 175 and 1,900 m structurally below the base of the Greater Himalayan series. The major mineral assemblages in the samples collected from the Modi Khola valley record only one episode of metamorphism to the garnet zone or higher grades, although previously reported ca. 500 Ma concordant monazite inclusions in some Greater Himalayan garnets indicate pre-Cenozoic metamorphism.

Keywords Himalaya · Tectonics · Thermobarometry · Metamorphism · Inverted metamorphism

Introduction

Metamorphic rocks are widely exposed in the Himalaya, leading some of the first geologists exploring the range to realize their importance in the formation of the thrust belt (Hooker 1854; Mallet 1874; Middlemiss 1887). Some early workers also recognized that the relationships between the metamorphic rocks and the faults and ductile shear zones that cut them are critically important for understanding the processes that created the Himalaya (Mallet 1874; Heim and Gansser 1939). Many subsequent studies have focused on Himalayan metamorphic rocks, particularly the highest grade rocks exposed in the thrust belt, the Greater Himalayan series. These rocks currently are exposed along a strip in the geographic interior of the orogen, where they rest structurally above Lesser Himalayan strata along the Main Central thrust (MCT; Fig. 1). With few exceptions, most workers find increasingly high-grade rocks exposed at progressively higher structural levels in the frontal half of the thrust belt, between the Main Frontal thrust and the South Tibetan Detachment System (STDS; Hooker 1854; Mallet 1874; Macfarlane 1995; Stephenson et al. 2000;

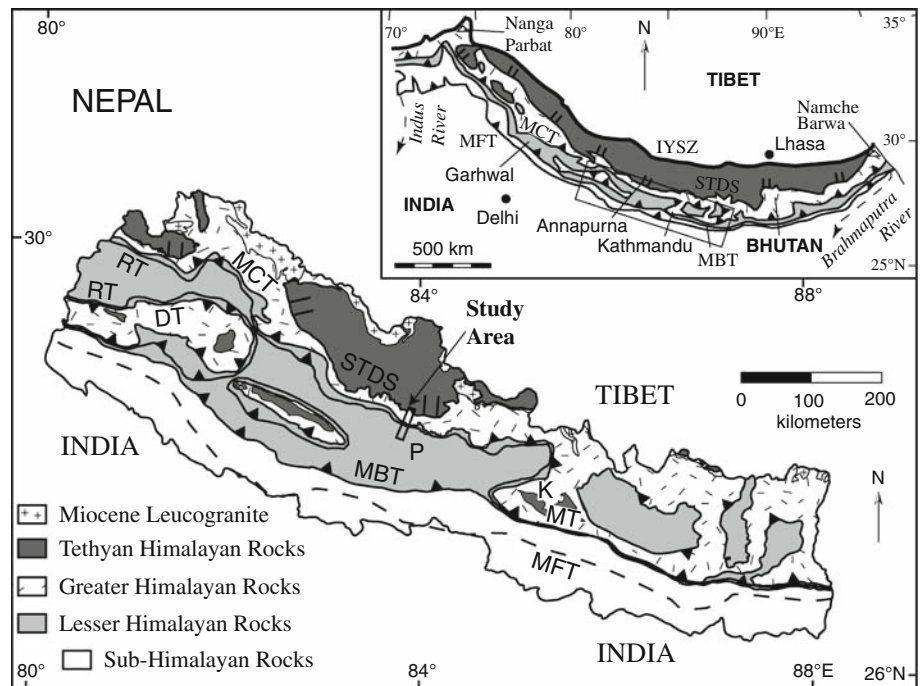
Communicated by T.L. Grove.

Electronic supplementary material The online version of this article (doi:10.1007/s00410-009-0424-3) contains supplementary material, which is available to authorized users.

A. J. Martin (✉)
Department of Geology, University of Maryland,
College Park, MD 20742, USA
e-mail: martinaj@geol.umd.edu

J. Ganguly · P. G. DeCelles
Department of Geosciences, University of Arizona,
Tucson, AZ 85721, USA

Fig. 1 Generalized geologic map of Nepal modified from Amatya and Jnawali (1994). *K* Kathmandu, *P* Pokhara. Inset: Highly generalized geologic map of the Himalayan orogen from Sorkhabi and Macfarlane (1999). *IYSZ* Indus-Yarlung Suture Zone, *STDS* South Tibetan Detachment System, *MCT* Main Central thrust, *DT* Dadeldhura thrust, *MT* Mahabarat thrust, *RT* Ramgarh thrust, *MBT* Main Boundary thrust, *MFT* Main Frontal thrust



Catlos et al. 2001; Daniel et al. 2003; Dasgupta et al. 2004; 2009; Goscombe et al. 2006). This spatial pattern of exposed metamorphic rocks has been termed inverted metamorphism, and explanations for the pattern are critical features of kinematic and dynamic models of the tectonic evolution of the Himalayan thrust belt (e.g. Jamieson et al. 1996; Guillot 1999; Harrison et al. 1999). These models include elements such as ductile extrusion in a mid-crustal channel (e.g. Jain and Manickavasagam 1993; Grujic et al. 2002; Jamieson et al. 2004; Harris 2007; Faccenda et al. 2008; Dasgupta et al. 2009), heating due to motion on major thrust-sense ductile shear zones (e.g. Le Fort 1975; England et al. 1992; Harrison et al. 1997), and critical taper (e.g. Robinson et al. 2003; Yin 2006; Webb et al. 2007; Kohn 2008).

Although some previous workers examined the metamorphic petrology of the strata in the Modi Khola transect (Arita 1983; Paudel and Arita 2000; Beyssac et al. 2004; Bollinger et al. 2004, and references therein), no quantitative pressure estimates were published for this area. However, there are published pressure and temperature estimates from a transect to the west along the Kali Ghandaki river and one to the east along the Marsyangdi river. In the Kali Ghandaki transect, Vannay and Hodges (1996) estimated that most Greater Himalayan rocks experienced pressures of 6–11 kbar at temperatures between 500 and 650°C. In the Marsyangdi valley, Catlos et al. (2001) determined pressures of 6–8 kbar at 450–550°C for Lesser Himalayan rocks and 8–12 kbar at 600–750°C for Greater Himalayan rocks. Some previous studies in the southern Annapurna Range concluded that two

episodes of metamorphism to the garnet zone or higher grades affected Greater and/or Lesser Himalayan rocks during the Cenozoic Himalayan orogeny, although these two events may simply be a prograde followed by a retrograde metamorphism (Pecher 1989; Vannay and Hodges 1996; Paudel and Arita 2000). In this paper we provide new pressure and temperature estimates for Greater and Lesser Himalayan rocks in the Modi Khola transect and evaluate the interpretation of multiple metamorphic episodes based on new petrologic data.

Recent advances in understanding the stratigraphy and structure of Lesser Himalayan deposits in Nepal (Upreti 1996; DeCelles et al. 2001; Dhital et al. 2002; Pearson and DeCelles 2005), in documenting the chemical differences between Greater and Lesser Himalayan strata (Ahmad et al. 2000; DeCelles et al. 2000, 2004; Robinson et al. 2001; Gehrels et al. 2003; Martin et al. 2005), and in estimating the spatial distribution of strain in rocks near the MCT (Martin et al. 2005) allow us to map the locations of the MCT as well as previously unrecognized faults in Lesser Himalayan strata with unprecedented accuracy. Our new mapping in the Modi Khola valley of the southern Annapurna Range in central Nepal affords an excellent opportunity to assess the spatial pattern of exposed metamorphic rocks in a well-constrained structural setting. The combination of thermobarometry and structural geometry shows that large displacement thrust-sense and normal-sense faults and ductile shear zones mostly control the pattern of exposed metamorphic rocks. Peak pressure and temperature estimates, and, critically, their spatial relationships with faults and ductile shear zones, are important

parts of most tectonic models and are required to fully evaluate the models.

Geologic setting

Greater and Lesser Himalayan metasedimentary strata are exposed in a broad swath in the center of the Himalayan fold-thrust belt (Fig. 1). Following Le Fort (1975) and Searle and Godin (2003), we divide the Greater Himalayan series in central Nepal into a lower pelitic, semi-pelitic, and psammitic unit, Unit I, and an upper calcareous unit, Unit II (Fig. 2). These strata may be the amphibolite facies equivalents of the lower formations of the structurally higher Tethyan series (Le Fort 1975; Gehrels et al. 2003; Myrow et al. 2003). For individual Unit I quartzite and schist samples, the youngest ages recorded by multiple detrital zircons are in the range 900–640 Ma (Parrish and Hodges 1996; Gehrels et al. 2003; Martin et al. 2005). Unit III, a ca. 500 Ma felsic orthogneiss, intrudes Unit II (Hodges et al. 1996). These dates constrain the depositional age of the Greater Himalayan protoliths to the Neoproterozoic to Cambrian. Ductile thrust and normal faults internally shortened and extended Greater Himalayan rocks (Reddy et al. 1993; Hodges et al. 1996; Kohn et al. 2004).

The structural top of the Greater Himalayan series is the STDS, a group of 2–3 moderately north-dipping normal faults and ductile shear zones with cumulative slip of many tens of kilometers (Fig. 1; Burchfiel et al. 1992; Searle et al. 2003). The STDS places Tethyan metasedimentary deposits on Greater Himalayan metasedimentary strata. Tethyan rocks occupy the northern half of the thrust belt, stretching from the STDS to the Indus-Yarlung suture zone, the site of the former subduction zone between Indian oceanic lithosphere and Asia (Fig. 1; Burg and Chen 1984; Ratschbacher et al. 1994; Murphy and Yin 2003).

The structural base of the Greater Himalayan series is the MCT, a top-to-the-south ductile shear zone that places Greater Himalayan metasedimentary strata on less-metamorphosed Lesser Himalayan metasedimentary formations (Fig. 1). We use the location of the MCT given by Martin et al. (2005), who map the MCT at the location of greatest strain within the ductile shear zone and find that this location exactly matches the protolith boundary between Greater and Lesser Himalayan strata. The MCT accommodated at least 160 km of slip (Pearson 2002; see also Robinson 2008).

Lesser Himalayan rocks are cut by numerous major thrust faults, most importantly the Ramgarh thrust (Fig. 1). In Nepal, the Ramgarh thrust accommodated at least 120 km of shortening and is the roof thrust for a large Lesser Himalayan duplex (DeCelles et al. 2001; Pearson and DeCelles 2005; Robinson et al. 2003, 2006; Robinson

2008). The lower part of the Lesser Himalayan series, the Nawakot Unit, mostly consists of Paleo- and Mesoproterozoic metamorphosed sandstones, muddy sandstones, and shales (Upreti 1996; DeCelles et al. 2000, 2001; Dhital et al. 2002). Two thick meta-carbonate formations are present near the top of the Nawakot Unit. The upper part of the Lesser Himalayan series, the Tansen Unit, consists of clastic Carboniferous to Paleocene Gondwanan strata and Eocene to lower Miocene Himalayan foreland basin deposits (Sakai 1983; Upreti 1996; DeCelles et al. 1998a, 2004).

The structural base of the Lesser Himalayan series is the Main Boundary thrust, which places Lesser Himalayan metasedimentary rocks on Sub-Himalayan strata (Fig. 1). The Sub-Himalayan series is composed entirely of Neogene Siwalik Group foreland basin deposits (Mugnier et al. 1993; Quade et al. 1995; DeCelles et al. 1998b). Several thrusts repeat parts of the Siwalik Group, and the Main Frontal thrust juxtaposes the Siwaliks against Quaternary alluvium along the front of the Himalayan range (Fig. 1; Powers et al. 1998; Lave and Avouac 2001).

Geology in Modi Khola valley

All rocks in the study area are pervasively foliated and most are lineated. Lesser Himalayan rocks are finer grained and lower grade than Greater Himalayan rocks. Greater Himalayan strata within about 200 m above the MCT are more micaceous and thus more schistose than structurally higher gneisses. Strain caps, strain shadows, and rotated inclusion trails indicate that all the garnets used for pressure–temperature determinations grew before or during deformation of their host rock.

Large displacement thrust-sense and normal-sense faults and ductile shear zones dominate the structural geometry of the Modi Khola valley (Fig. 2; Hodges et al. 1996). In this paper we follow the mapping of Hodges et al. (1996), Searle and Godin (2003), Pearson and DeCelles (2005), and Martin et al. (2005), modified to match our more recent observations on both sides of the Modi Khola valley. Foliations dip about 30° north in the hanging wall and footwall strata of the MCT, which probably has a hanging wall flat on footwall flat geometry (Figs. 2, 3; Pearson and DeCelles 2005; see also Webb et al. 2007; Robinson 2008). The Ramgarh thrust also cuts Lesser Himalayan deposits in the study area. By analogy with balanced cross-sections near Kathmandu in central Nepal, in far western Nepal, and in Kumaun, India, we infer that the Ramgarh is the roof thrust for a large duplex composed of Lesser Himalayan rocks (Srivastava and Mitra 1994; DeCelles et al. 2001; Pearson and DeCelles 2005; Robinson et al. 2003, 2006; Robinson 2008). Growth of this duplex passively tilted both the Lesser and Greater Himalayan rocks above it and

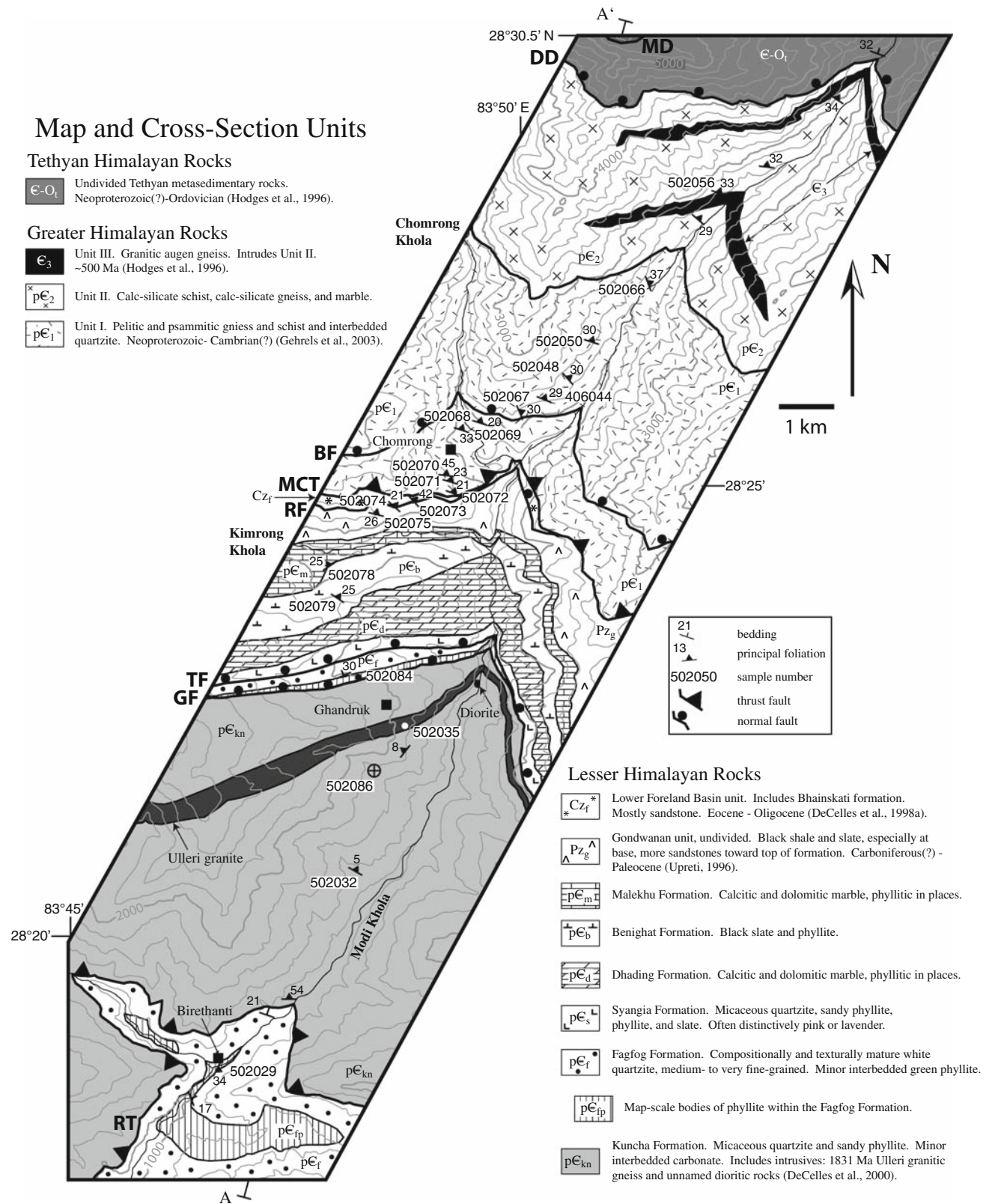


Fig. 2 Geologic map of the Modi Khola transect. Strike-and-dip symbols show the location of samples, except for samples 502035 and 502084, for which locations are given by circles. *BF* Bhanuwa fault, *DD* Deorali detachment, *GF* Ghandruk fault, *MCT* Main Central thrust, *MD*

Macchapucchare detachment, *RF* Romi fault, *RT* Ramgarh thrust, *TF* Tobro fault. Geology north of Deorali detachment from Hodges et al. (1996). Modified from Martin et al. (2005) and references therein to match our more recent observations. Contours: 200 m

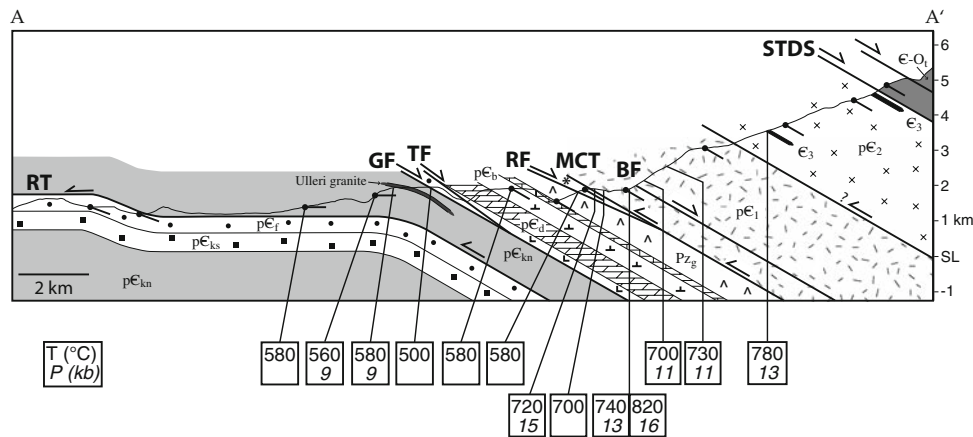


Fig. 3 Schematic (not balanced) cross-section for the Modi Khola transect. Peak metamorphic conditions are about the same in each block bounded by major faults or ductile shear zones but recorded conditions change dramatically across faults or shear zones with large slip. Location of cross-section, lithologic units, and abbreviations given in Fig. 2 except the Kushma Formation, labeled pE_{kn} , which

the faults and ductile shear zones contained within these strata to their current approximately 30° north-dipping attitudes.

Several normal-sense faults and ductile shear zones with large displacements crop out within the study area (Figs. 2, 3). The Deorali and Macchhapuchhare detachments are strands of the STDS (Hodges et al. 1996). In this paper we present evidence for a large normal fault in Greater Himalayan strata, the Bhanuwa fault. Another normal fault, the Romi fault, lies directly below the MCT and juxtaposes Lesser Himalayan Eocene–Miocene foreland basin deposits against Gondwanan strata (modified from Martin et al. 2005). The Tobro fault is a structurally lower normal fault within Lesser Himalayan rocks that places the Syangia Formation on the Fagfog Formation, and the structurally related Ghandruk fault is a normal fault that places the Fagfog and Syangia on the Kuncha Formation (note that our revised stratigraphy and mapping shows that the Ghandruk fault is a normal fault, not a thrust as indicated by Martin et al. 2005). Slip on some parts of the STDS was synchronous with motion on the MCT (Hodges et al. 1996; Searle and Godin 2003). Searle and Godin (2003) conclude that slip on the Macchhapuchhare detachment was approximately synchronous with slip on the MCT, and that slip on both faults is younger than slip on the Deorali detachment.

Methods

Electron microprobe analysis

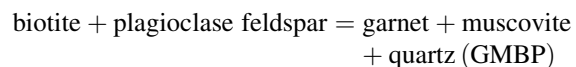
We present analyses of 21 samples of chlorite- to kyanite-zone rocks collected along a 25 km traverse in the Modi

sits stratigraphically between the Kuncha and Fagfog Formations. The Fagfog Formation is shown undivided. Tadpoles show dip of bedding or metamorphic foliation. Structural style similar to balanced cross-sections by DeCelles et al. (2001), Pearson (2002), and Robinson et al. (2003, 2006)

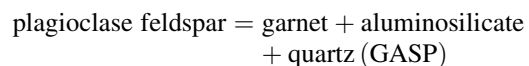
Khola valley (Fig. 2). Mineral identification and microstructural characterization were performed using an optical petrographic microscope. We determined mineral compositions by spot analysis with the Cameca SX-50 electron microprobe at the University of Arizona. Standards and operating conditions are given in Table S1. We also measured concentrations of F and Cl in biotite and muscovite using the microprobe. The method for calculating F and Cl mole fractions is given at the bottom of Table S2.

Thermobarometry

We estimated peak temperatures using the garnet–biotite and garnet–ilmenite cation exchange thermometers. We estimated the pressure at peak temperature using barometers based on the equilibria:



and



The GASP barometer was applied only to Unit I samples structurally above the Bhanuwa fault (502050 and 502067) because only these samples contain an aluminosilicate phase (kyanite). When possible, we averaged several individual microprobe analyses to obtain a representative composition for each mineral used for the temperature and pressure estimates. Strategies for selecting appropriate mineral compositions to provide the best estimate of peak conditions are discussed in a separate section.

We used the garnet–biotite and GASP formulations written by Ganguly and Cheng into a computer program that calculates temperatures and pressures given mineral composition inputs (available at ftp://ftp.geo.arizona.edu/pub/ganguly/P-T_Calc/GtBt-GASP/). For the garnet–biotite thermometer, the program uses the experimental data of Ferry and Spear (1978) in the Fe–Mg binary system and the mutually compatible biotite and garnet solution models of Ganguly et al. (1996a). For the GASP barometer, the program uses the experimental data of Koziol and Newton (1989) for the end-member reaction, the garnet solution model of Ganguly et al. (1996a), and the plagioclase solution model of Elkins and Grove (1990). Fe^{3+} contents were estimated as 3 mol% of total Fe in garnet and 11.6 mol% of total Fe in biotite based on the average values for pelites used by Holdaway et al. (1997). For garnet, these Fe^{3+} contents closely match estimates based on charge balance. The assumption that all Fe is Fe^{2+} would increase the temperature estimates by about 25°C for the lower grade rocks and by about 40°C for the higher grade rocks. In two studies of metamorphism in Sikkim, the thermobarometric formulations we used in this work were shown to yield pressure and temperature estimates that are more consistent with independent constraints from mineral assemblages (Dasgupta et al. 2004) and the spatial trend of estimated temperatures suggested by prograde homogenization of compositional zoning in garnet (Dasgupta et al. 2009), than other approaches, including the widely used average P – T method (Holland and Powell 1998).

We corrected estimated temperatures for F and Cl in biotite using the formulation of Zhu and Sverjensky (1992; see Table 1 for a summary of the F data). These corrections resulted in a net increase in the temperature estimate of 15–30°C for all samples except 502056 (+41°C) and 502074G (+70°C). We tested the effect of correcting biotite compositions for retrograde modification using the method of Kohn and Spear (2000). Because the area of garnet is small and the area of biotite is large in all thin sections, the correction to the biotite composition was small for each sample, resulting in a temperature change of a few degrees. Thus we do not correct for retrograde modification of the composition of biotite.

We applied the garnet–ilmenite thermometer only to Lesser Himalayan rocks. Only ilmenite inclusions in garnet were used for garnet–ilmenite thermometry. Temperatures were calculated using the equation:

$$T(K) = \frac{14,642 - 2,200(2X_{\text{Mn}}^{\text{ilm}} - 1) + 539(X_{\text{Mn}}^{\text{grt}} - X_{\text{Fe}}^{\text{grt}}) + 12,083X_{\text{Mg}}^{\text{grt}}}{R \ln K_D + 7.67X_{\text{Mg}}^{\text{grt}} + 4.203}$$

X_{Mn} is the mole fraction of Mn, defined as $\text{Mn}/(\text{Fe}^{2+} + \text{Mg} + \text{Ca} + \text{Mn})$, X_{Fe} and X_{Mg} are defined analogously, ilm is ilmenite, grt is garnet, R is the gas constant in units of joules per mole per Kelvin, and K_D is the equilibrium Fe–Mn distribution coefficient between garnet and ilmenite, defined as the ratio $(\text{Fe}/\text{Mn})^{\text{ilm}}/(\text{Fe}/\text{Mn})^{\text{grt}}$. This equation uses the experimental calibration for the binary system by Pownceby et al. (1991), the modification of that formulation by Ganguly et al. (1996b), and a correction for Mg in garnet using the garnet solution model of Ganguly et al. (1996a). Corrections for Ca in garnet and for pressure were very small and were omitted.

We used the formulation of the GMBP barometer by Hoisch (1990), corrected by Hoisch (1991). In order to estimate pressure, we used the mean value from the clusters of crossings of GMBP equilibria closest to the garnet–biotite exchange equilibrium (Fig. 4). Dasgupta et al. (2004) conclude that pressures estimated using the GASP barometer are more consistent with constraints from phase equilibria than GMBP estimates.

Uncertainties

One type of uncertainty in thermobarometric calculations is absolute error, or accuracy, which is the difference between the estimated pressure or temperature and the conditions actually experienced by the rock. This type of error includes inherently non-random elements such as uncertainty about which compositions in heterogeneous minerals represent desired equilibrium conditions (Kohn and Spear 1991). Absolute error is typically large, at least ± 75 – 100°C and ± 1 – 3 kbar (Hodges and McKenna 1987; Kohn and Spear 1991). A second type of error is the uncertainty of one thermobarometric estimate relative to another. Relative error is usually smaller than absolute error and can be significantly reduced by comparing estimates using the same barometer or thermometer. In this paper, we only compare pressures estimated with the GMBP barometer and mostly compare temperatures estimated with the garnet–biotite exchange thermometer. However, because of the absence or scarcity of biotite in some Lesser Himalayan samples, we are forced to compare garnet–ilmenite temperature estimates from samples 502079, 502084, and three of four garnets from 502032 with garnet–biotite temperature estimates from the other samples. We estimate relative errors for our samples as $\pm 35^\circ\text{C}$ and ± 1 kbar (2-sigma) based on the estimates of Hodges and McKenna (1987), Kohn and Spear (1991), Holdaway and Mukhopadhyay (1993), and Todd (1998). These uncertainties mean that we can confidently distinguish temperature and pressure differences between samples greater than 35°C and 1 kbar.

Table 1 Sample locations and fluorine contents

Sample number	Lithologic unit	Latitude ^a °N	Longitude ^a °E	Structural distance above top of Fagfog formation (m) ^b	Biotite mean X_F	Measurements
Deorali detachment				7,775		
502056	Unit III granite	28.47078	83.86903	6,250	0.066	4
Fm II boundary				5,575		
502066	Unit I	28.45531	83.85773	5,550	0.025	3
502050	Unit I	28.44343	83.84626	4,825	0.023	3
502048	Unit I	28.43733	83.84215	4,525	0.020	3
502067	Unit I	28.43072	83.83379	4,475	0.022	3
Bhanuwa fault				4,425		
502068	Unit I	28.42828	83.82593	4,350	0.041	4
502069	Unit I	28.42710	83.82279	4,275	0.038	3
502070	Unit I	28.41865	83.82009	3,950	0.041	3
502071	Unit I	28.41742	83.82075	3,900	0.025	3
502072	Unit I	28.41510	83.81734	3,775	0.015	4
MCT				3,750		
502073	Lower foreland	28.41370	83.81438	3,645	0.041	3
502074G	Lower foreland	28.41244	83.81131	3,577	0.144	4
Romi fault				3,575		
502075	Gondwanan	28.41222	83.80651	3,500	0.102	3
502078	Benighat	28.40166	83.79812	2,900	0.067	3
502079	Benighat	28.39588	83.79992	2,625	^c	0
Tobro fault				2,050		
502084	Fagfog	28.38115	83.80532	1,850	No bt	0
Ghandruk fault				1,840		
502035U	Ulleri granite	28.37224	83.81196	1,155	0.090	3
502035S	Kuncha	28.37224	83.81196	1,150	0.056	3
502086	Kuncha	28.36395	83.80640	1,000	0.040	9
502032	Kuncha	28.34515	83.80319	700	0.028	3
Ramgarh thrust				0		
502029	Fagfog	28.30905	83.77748	−200	0.042	3

In case of discrepancy, locations on map supersede GPS

^a Map datum: India Bangladesh. GPS locations can be inaccurate by tens of meters

^b Structural distances are for the deformed state. Refers to the southern exposure of the Fagfog formation

^c We did not measure the F content of the sparse biotite in sample 502079

Mineral assemblages

Most Lesser Himalayan semi-pelites in the study area contain the peak equilibrium assemblage quartz + muscovite + biotite ± garnet ± plagioclase feldspar (Fig. 5). Exceptions are sample 502029, which does not contain muscovite, and sample 502084, which contains chlorite but no biotite. Accessory phases include graphite, tourmaline, ilmenite, pyrite, allanite, apatite, clinozoisite, rutile, magnetite/hematite, titanite, zircon, monazite, thorite/huttonite, and thorianite. Most samples also contain retrograde chlorite.

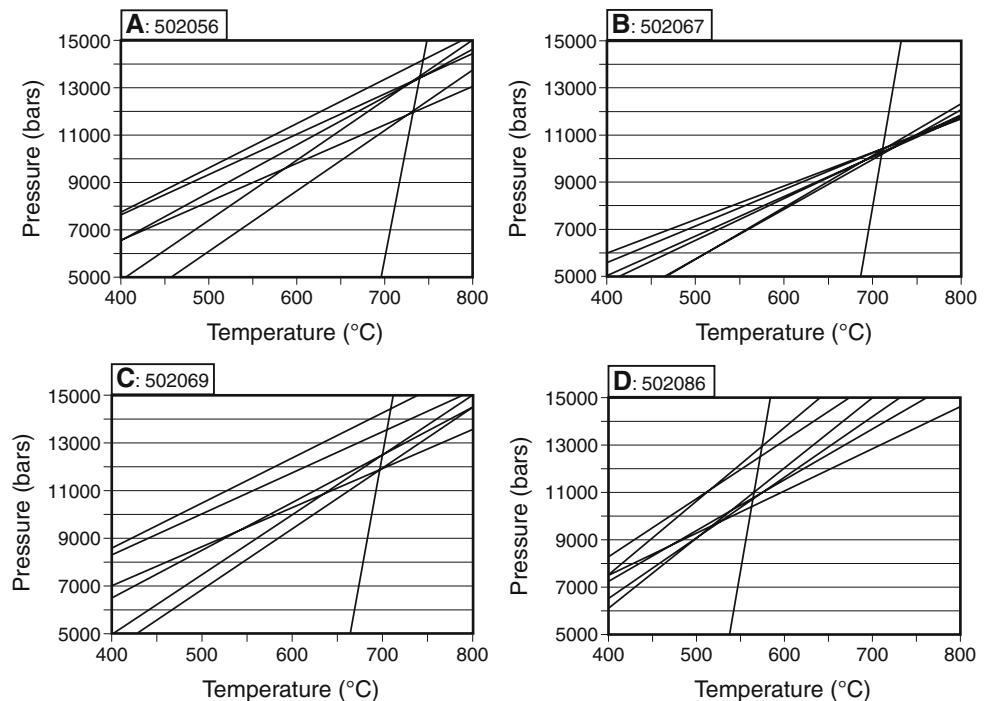
Most Greater Himalayan semi-pelites between the MCT and the Bhanuwa fault contain the peak assem-

blage quartz + muscovite + biotite + plagioclase + garnet (Fig. 5). However, sample 502072 contains both paragonite and muscovite and sample 502070 does not contain plagioclase. Accessory minerals are tourmaline, ilmenite, rutile, allanite, apatite, magnetite/hematite, monazite, zircon, pyrite, xenotime, and thorianite.

Unit I semi-pelites north of the Bhanuwa fault contain the peak assemblage quartz + muscovite + biotite + plagioclase ± garnet ± kyanite (Fig. 5). Thus an aluminosilicate phase first enters the peak assemblage about 1 km structurally above the MCT. Accessory minerals include tourmaline, rutile, apatite, barite, zircon, monazite, and xenotime.

Unit III, a metamorphosed granite, contains the assemblage plagioclase + quartz + muscovite + biotite + garnet.

Fig. 4 The six GMBP equilibria (gentle slopes) and the garnet–biotite Fe–Mg exchange equilibrium (steep slope) for mineral compositions from **a** Greater Himalayan Unit III granite sample 502056; Greater Himalayan metasedimentary samples **b** 502067 and **c** 502069; and **d** Lesser Himalayan metasedimentary sample 502086. These equilibria are shown for the peak metamorphic conditions recorded by the minerals in each rock



Unit III rocks also contain potassium feldspar, which probably is of igneous origin and not a part of the peak metamorphic assemblage. Accessory phases include zircon and monazite.

All sampled Greater Himalayan Unit I and Unit III rocks contain retrograde chlorite. We did not find staurolite or sillimanite in any samples, consistent with the findings of Hodges et al. (1996). All garnets used for thermobarometry show microstructural evidence for growth before or during deformation such as foliation deflection, strain caps, strain shadows, and inclusion trail rotation (see Fig. 5, e.g., see also Martin 2009).

Mineral compositions and major element zoning

We measured two different patterns of zoning of major elements in garnet crystals in contact with biotite in semi-pelites from the Modi Khola transect. Petrologic interpretations and compositional variations within and between grains determine which composition within a garnet should be combined with which composition of ilmenite, biotite, muscovite, and plagioclase to obtain the best estimate of the peak temperature and the pressure at that temperature.

Measurements

Several examples of the two patterns of major element zoning in garnet crystals are shown as profiles in Fig. 6 and as X-ray maps in Fig. 7. Garnet sizes can be measured from these figures and the images in Fig. 5. Selected

compositions are given in Table S3. The two types of zoning are as follows:

1. Monotonically decreasing X_{Mn} values from the core to the rim of the garnet (Figs. 6e, 7e). This pattern is present in garnets in contact with biotite in all of the Lesser Himalayan samples. The pattern of decreasing X_{Mn} values from core to rim is also present at a much larger scale in garnets from Unit I samples 502070 and 502071 (Fig. 6). These garnets show minor reversal of this pattern, an increase in X_{Mn} of 0.01, within a few microns of the rim.
2. Nearly flat profiles for all major elements in the core of the garnet with upturns in X_{Mn} , X_{Fe} , and $Fe/(Fe + Mg)$ values, and a corresponding downturn in the X_{Mg} value, toward the rim of the garnet (Figs. 6a–d, 7a–d). Figure 6 shows that the magnitude and the spatial extent of the excursions near the rim vary between samples.

Ilmenite, biotite, muscovite, and most plagioclase crystals are not appreciably zoned, although in some samples the compositions of these minerals vary with location relative to garnet grains. Some, but not all, plagioclase crystals in Greater Himalayan samples 502050 and 502068 have rims with slightly elevated Ca concentrations compared to their cores. Plagioclase in the other samples is not appreciably zoned.

In Lesser Himalayan rocks, ilmenite inclusions near the cores of garnets usually contain more Mn than ilmenite inclusions near the rims. Garnet near ilmenite inclusions is not appreciably zoned.

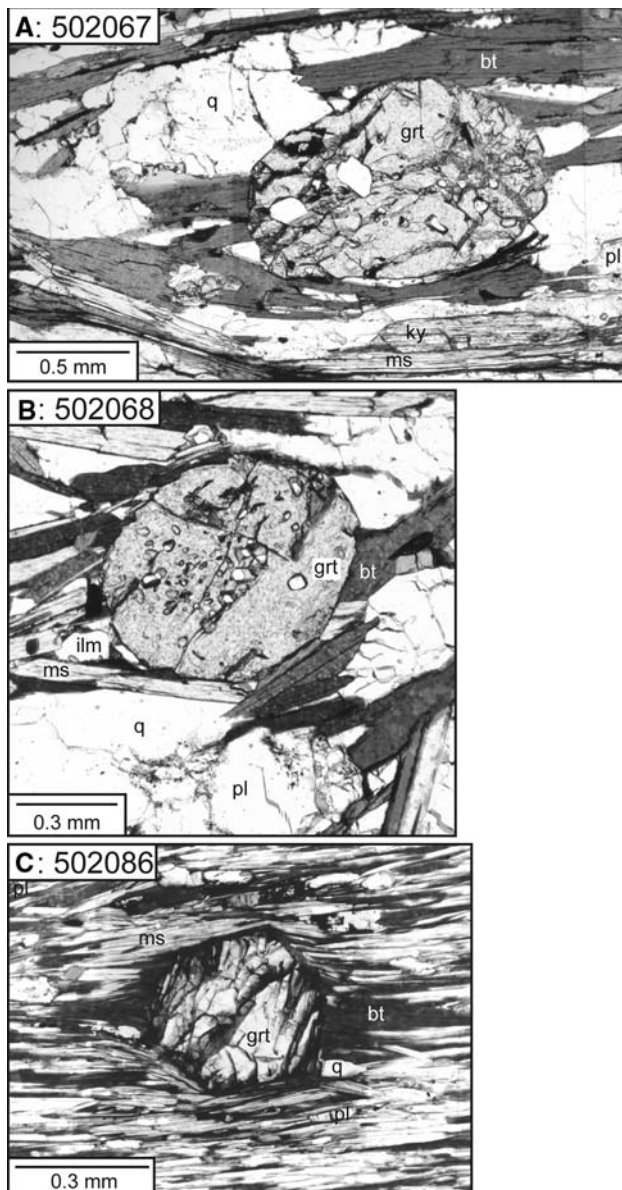


Fig. 5 Images showing peak assemblages. **a** Photomicrograph of garnet from Greater Himalayan Unit I sample 502067 from the hanging wall of the Bhanuwa fault. Rocks in the hanging wall of the Bhanuwa fault contain kyanite whereas rocks in the footwall do not. Thus the first appearance of an aluminosilicate mineral is at the location of the Bhanuwa fault, about 1 km structurally above the MCT. Deflection of foliation at the bottom of the garnet rules out post-kinematic growth of this garnet. **b** Photomicrograph of garnet from Unit I sample 502068 from between the MCT and the Bhanuwa fault. **c** Photomicrograph of garnet from Lesser Himalayan sample 502086. Deflection of foliation and strain shadows composed of biotite rule out post-kinematic growth of this garnet. All photographs taken in plane light. *bt* biotite, *grt* garnet, *ilm* ilmenite, *ky* kyanite, *ms* muscovite, *pl* plagioclase feldspar, *q* quartz

Interpretations of garnet zoning

We interpret the two patterns of major element zoning in garnet crystals in semi-pelites from the Modi Khola valley

using results from numerical modeling and from natural and synthetic garnets discussed by Ganguly and Saxena (1987) and Spear (1995).

1. The patterns of monotonically decreasing X_{Mn} values toward the rim of these garnets are growth zoning profiles, produced during the growth of the garnet. The small magnitude, limited extent upturns of X_{Mn} values at the rims of some of the garnets are the result of limited retrograde modification of the composition at the rim of the garnet and diffusion of elements within the garnet crystal.
2. The flat profiles in the cores of these garnets indicate that growth zoning profiles were completely relaxed and the distributions of major elements in the garnets were homogenized during high-temperature metamorphism. As for zoning type 1, the upturn in X_{Mn} , X_{Fe} and $Fe/(Fe + Mg)$ values and the corresponding downturn in the X_{Mg} value toward the rims of the garnets result from retrograde modification of the composition at the rim and diffusion of elements within the garnet crystal.

Dissolution of garnet on the prograde path also can generate upturns in Mn concentrations at the rims of garnets. Prograde production of the X_{Mn} upturns in our samples is unlikely for several reasons. First, the flat profiles in the cores of garnets from samples 502050 to 502071 indicate complete homogenization of growth zoning in the interior of the grains. There is no reasonable geologic scenario whereby prograde growth zoning is homogenized in the interior of garnet crystals yet at least partially retained at the rims. Second, the most common prograde reactions involving breakdown of garnet produce staurolite or aluminosilicate, but none of our samples contain staurolite and only samples 502050 and 502067 contain an aluminosilicate phase. In these samples, kyanite is distributed throughout the rock, is not spatially associated with garnet grains, and is parallel to foliation (Fig. 5a), suggesting limited importance of garnet breakdown for kyanite growth. Garnets that crystallize from a cooling melt can also have Mn concentration upturns near their rims (Spear 1995), but there is no evidence for melt in the semi-pelites nor for Cenozoic melting of the ca. 500 Ma Unit III meta-granite nor the ca. 1,831 Ma Ulleri meta-granite (DeCelles et al. 2000).

Strategies for selecting compositions for thermobarometry

For the two types of zoning profiles in garnet, we use the following combinations of mineral compositions to estimate peak temperatures and corresponding pressures.

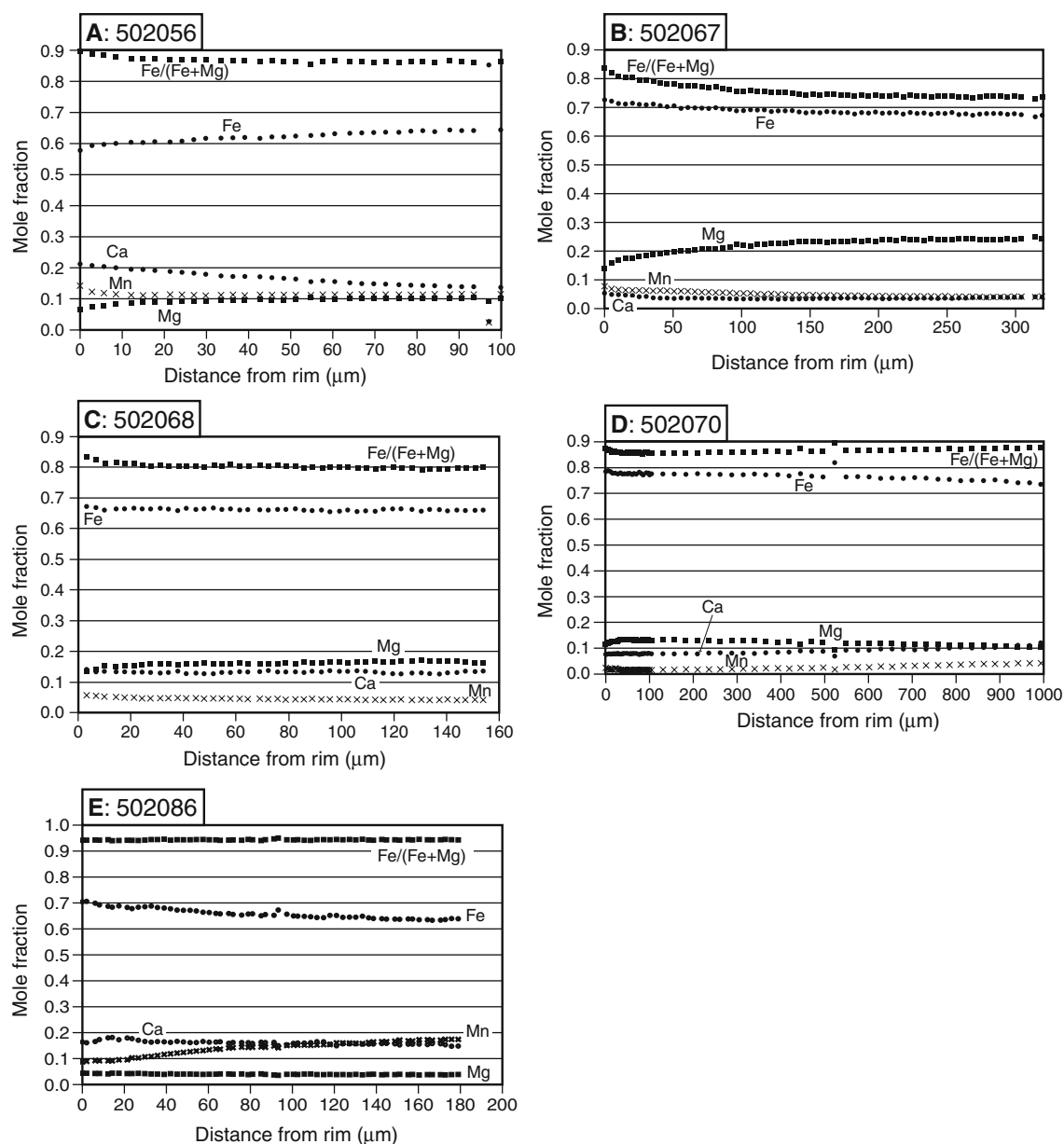


Fig. 6 Profiles of major element compositions of garnets from **a** Greater Himalayan Unit III granite sample 502056; Greater Himalayan metasedimentary samples **b** 502067, **c** 502068, and **d** 502070; and **e** Lesser Himalayan metasedimentary sample 502086. Profiles cover the region from the core of the garnet to a rim, where the garnet touches biotite. Note the different scales. Locations of the

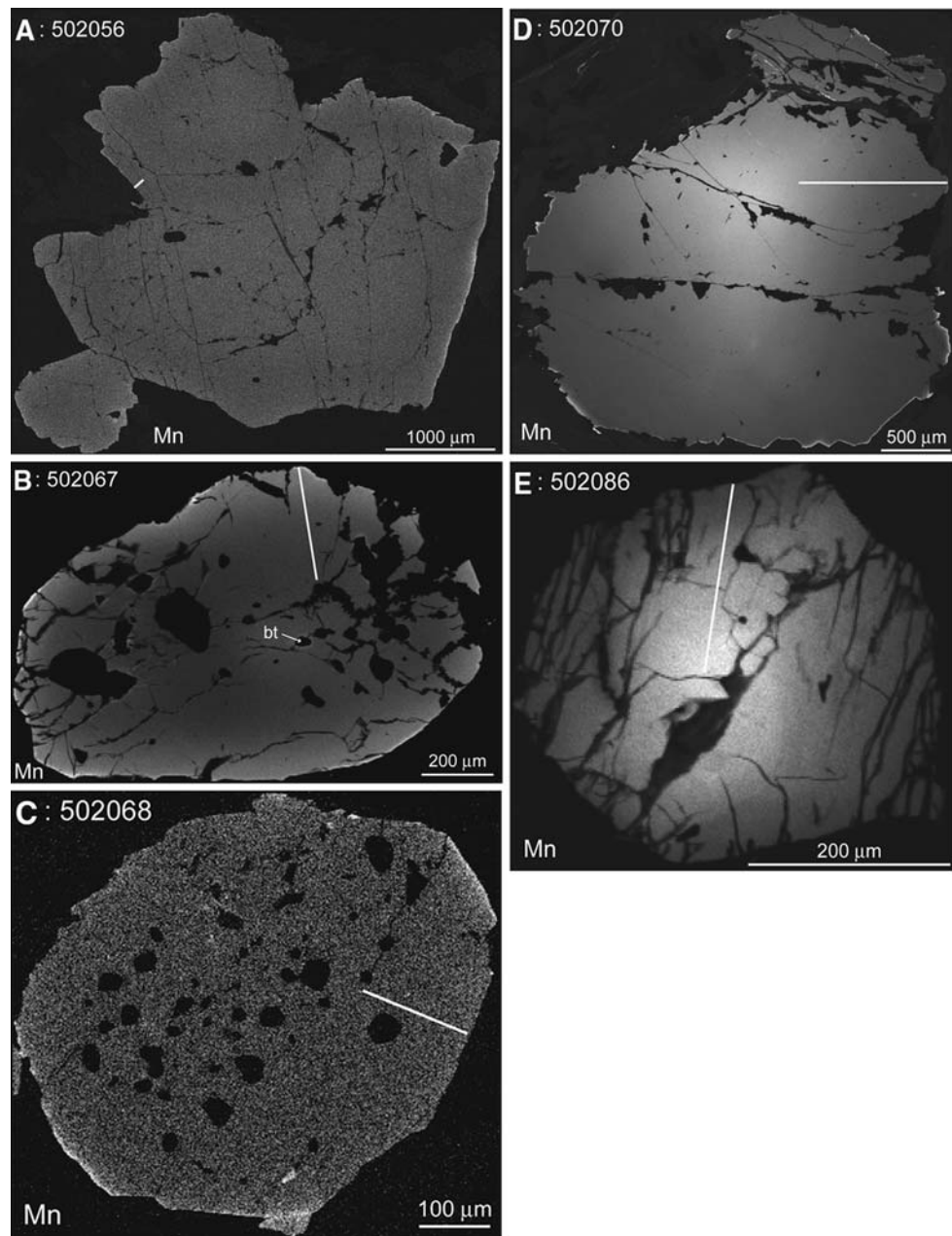
Garnets that preserve growth zoning

The composition of garnet that most closely preserves peak metamorphic conditions is the composition nearest the rim that is still unaffected by retrograde reactions. We use this composition of garnet for garnet–biotite thermometry and for GMBP barometry. For Lesser Himalayan rocks (samples 502032, 502086, and 502035S), we combine this garnet composition with the compositions of biotite, muscovite, and plagioclase as close to the garnet as

profiles are shown in Fig. 7. Samples 502070 and 502086 preserve growth zoning with some retrograde modification near the rim whereas samples 502056, 502067, and 502068 show compositional homogenization at high temperatures and retrograde modification near the rim. Note the dramatically different lengths of diffusion of retrograde modification into garnets from different samples

possible, taking care that the minerals used for thermo-barometry appear on the basis of textural relationships not to be retrograde products. As for the Lesser Himalayan samples, for Greater Himalayan samples 502070 and 502071, we use the composition of garnet nearest the rim that is unaffected by retrograde modification. However, for these samples, we combine this garnet composition with the compositions of biotite, muscovite, and plagioclase distal to the garnet crystal in order to reduce the effects of retrograde modification of these minerals.

Fig. 7 X-ray maps showing the Mn content of garnets from Greater and Lesser Himalayan rocks. *Bright areas* contain more Mn than dark areas. *White lines* show the locations of the profiles in Fig. 6. **a** 502056, **b** 502067, **c** 502068, **d** 502070, **e** 502086. The garnet composition near the biotite inclusion at the *center right* of the garnet from sample 502067 shows modification due to retrograde reaction with the biotite (*bt*)



For garnet–ilmenite thermometry, ilmenite inclusions near the rim of the garnet, but not in the portion of the rim affected by retrograde reactions, provide the best estimate of peak temperatures. We pair the ilmenite composition with a proximal garnet composition to obtain a temperature estimate.

Garnets with flat profiles in their cores and retrograde modification of their rims

In all cases, we use the core composition of garnet for garnet–biotite thermometry, GMBP barometry, and GASP barometry. We combine these core compositions with the

composition of biotite, muscovite, and plagioclase grains located distal to garnet grains to obtain estimates of peak temperatures and corresponding pressures.

For rocks that contain garnets with this zoning pattern, it is important to use large garnets for thermobarometry in order to minimize the possibility of resetting of core compositions during retrograde metamorphism. Ganguly and Tirone (1999) provide a method for determining whether the core of a mineral of a given size that cooled at a given rate was affected significantly by diffusion resulting from exchange with a surrounding homogeneous infinite matrix (e.g. biotite) during the cooling. They show that there is no significant resetting of the temperature

determined using the core composition of the mineral if the value of a dimensionless parameter, M , is ≤ 0.1 for a peak temperature $\leq 1,000^\circ\text{C}$. The parameter M is defined as

$$M = \frac{RD(T_0)T^2}{E\dot{T}a^2}$$

where R is the gas constant, $D(T_0)$ is the diffusion coefficient of the mineral at the peak temperature T_0 , E is the activation energy of diffusion, \dot{T} is the cooling rate at the temperature T , and a is the characteristic grain dimension (radius for a sphere or cylinder and half-length for a plane sheet). The cooling is assumed to follow a non-linear model given by $1/T = 1/T_0 + \eta t$, where η is a cooling time constant with dimension $\text{K}^{-1}\text{t}^{-1}$ and t is time. We use this equation to calculate the radius of a spherical garnet for $M = 0.1$ and a range of geologically reasonable cooling rates to determine the minimum radius of garnet to use for thermobarometry. For these calculations we use peak conditions of 10 kbar at 725°C . These conditions derive from the constraint that all Greater Himalayan samples except one contain the assemblage quartz + muscovite + plagioclase (sample 502070 does not contain plagioclase) and the maximum stability for this assemblage at 10 kbar is at approximately 725°C (Kerrick 1972; Le Breton and Thompson 1988).

We calculate the Fe^{2+} –Mg interdiffusion coefficient for garnet at the peak conditions using the self-diffusion data of Ganguly et al. (1998) and the relationship between the self- and interdiffusion coefficients of equally charged ionic species (Ganguly 2002). According to Hackler and Wood (1989), Fe^{2+} and Mg mix with a small positive deviation from ideality in garnet solid solution, so we make no correction for the effect of thermodynamic non-ideality in the calculation of the interdiffusion coefficient. We likewise do not make a correction for the effect of oxygen fugacity because Ganguly et al. (1998) conducted their experiments in graphite capsules that buffered the oxygen fugacity to conditions approximating those of pelites. This calculation yields an Fe^{2+} –Mg interdiffusion coefficient of $3.17 \times 10^{-19} \text{ cm}^2/\text{s}$ at 10 kbar, 725°C , and $\text{Fe}/(\text{Fe} + \text{Mg})$ of 0.8.

Using this interdiffusion coefficient for $D(T_0)$ in the above equation, $E = 66,000 \text{ cal/mol}$ (Ganguly et al. 1998), and a peak temperature of 725°C , we find that the core of a spherical garnet with radius >141 , >245 , and $>346 \mu\text{m}$ will not be reset ($M = 0.1$) for an initial cooling rate ≥ 15 , ≥ 5 , and $\geq 2.5^\circ\text{C/My}$, respectively. We estimate pressures and temperatures using the largest garnets in each thin section, preferably grains with radius greater than $346 \mu\text{m}$ to allow for possible very slow cooling of these rocks. All Greater Himalayan thin sections contain garnets with radii equal to or larger than $350 \mu\text{m}$ except sample 502050, for which we use a garnet with a radius of $275 \mu\text{m}$, and sample

502068, for which we use garnets with radii of 120 – $230 \mu\text{m}$ (Table 2). If the actual peak temperature were significantly hotter than 725°C and/or the actual initial cooling rate were significantly slower than 5°C/My for either sample then that sample likely provides a minimum estimate of peak conditions.

Our calculations of the minimum sizes of garnets needed to avoid resetting of core compositions during cooling differ significantly from the results of Spear (1991, 1995), who found that much larger garnets are required to prevent resetting for a given peak temperature and cooling rate. This discrepancy arises from the use of different diffusion data. Spear used data from experiments on tracer diffusion of ^{25}Mg in garnet by Cygan and Lasaga (1985), who conducted their studies at 2 kbar and high oxygen fugacity, near the hematite–magnetite buffer. Spear did not adjust the diffusion coefficient to a value appropriate for the oxygen fugacity and pressure conditions common in regionally metamorphosed pelites: oxygen fugacity near the graphite or quartz–fayalite–magnetite buffers and pressure of 5–10 kbar (the Arrhenius relation used by Spear was $D(\text{Mg}) = 9.8 \times 10^{-5} (\text{cm}^2/\text{s}) e^{-57098 (\text{cal/mol})/RT}$, where $D(\text{Mg})$ is the magnesium self-diffusion coefficient). Corrections for both effects would have substantially reduced the D value and hence the minimum grain size required to prevent resetting the core composition of garnets for a given cooling rate and peak temperature. In contrast to Spear (1991, 1995), we correct for the pressure effect and we also use self-diffusion data from the experiments of Ganguly et al. (1998), who maintained lower oxygen fugacity than Cygan and Lasaga (1985) through use of a graphite buffer. This lower oxygen fugacity is appropriate for the regional metamorphism of pelites. The resulting slower diffusion results in the calculation of smaller garnets necessary to avoid resetting of core compositions for a given peak temperature and cooling rate.

The $D(\text{Mg})$ value derived from Cygan and Lasaga (1985) at 2 kbar is much greater (by a factor of about 25 at 725°C) than that derived from Ganguly et al. (1998) at 10 kbar. However, as shown by the latter workers, the data are in very close agreement when corrections are made for the effects of oxygen fugacity and pressure. The quantitative oxygen fugacity and pressure effects on divalent cation diffusion coefficients in garnet were discussed first by Chakraborty and Ganguly (1991), who demonstrated the compatibility between Mg self-diffusion data that they obtained using spessartine–almandine diffusion couples and those of Cygan and Lasaga (1985) when corrections are made for the oxygen fugacity and pressure effects (as shown by Ganguly et al. (1998), Mg self-diffusion data are insensitive to garnet composition).

It follows from the above equation for M that the grain size required to prevent readjustment at the core of a

Table 2 Estimated peak conditions

Sample number	P (bar)	Number of estimates	Method	T (°C)	Number of estimates	Method	Garnet radii (μm)	Notes
Deorali detachment								
502056	13100	2	GMBP	780	2	Grt-Bt	450, 600	Meta-granite
Fm II boundary								
502050	10800	1	GMBP	730	1	Grt-Bt	275	GASP gives 10,700 bar
502067	10700	3	GMBP	700	3	Grt-Bt	350, 475, 730	GASP gives 10,400 bar
Bhanuwa fault								
502068	16100	3	GMBP	820	4	Grt-Bt	120, 130, 205, 230	
502069	13000	1	GMBP	740	1	Grt-Bt	900	
502070	No pl			700	2	Grt-Bt	840, 1,000	
502071	15000	2	GMBP	720	3	Grt-Bt	1,260, 2,000, 2,200	
MCT								
502074G	No pl			580	3	Grt-Bt		~70° correction for F
Romi fault								
502079	No pl			580	3	Grt-Ilm		Very little biotite
Tobro fault								
502084	No bt			500	2	Grt-Ilm		
Ghandruk fault								
502035S	8500	4	GMBP	580	5	Grt-Bt		
502086	9200	2	GMBP	560	4	Grt-Bt		
502032	No pl			580	4	Grt-Ilm		1 estimate using Grt-Bt
Ramgarh thrust								

Pressures are estimated at the peak temperature indicated; they likely are not peak pressures

Number of estimates means number of different mineral combinations

Relative errors between samples are approximately 1 kbar and 35°C at the 2-sigma level

Garnet radii provided only for Greater Himalayan samples because it is only for these samples that we use core compositions to estimate peak temperatures and corresponding pressures. Hence it is only for these samples that we must consider possible resetting of core compositions

GMBP garnet–muscovite–quartz–biotite–plagioclase feldspar barometer, *GASP* garnet–aluminosilicate–quartz–plagioclase feldspar barometer, *Grt–Bt* garnet–biotite Fe–Mg exchange thermometer, *Grt–Ilm* garnet–ilmenite Fe–Mn exchange thermometer

spherical crystal (determined by $M = 0.1$) scales as $\sqrt{D(T_0)/E}$. For the “uncorrected” Cygan and Lasaga (1985) data used by Spear (1991, 1995), this ratio is about 11 times greater than the value we obtain using the diffusion data of Ganguly et al. (1998), so the minimum grain size required to preserve the core composition of garnet during cooling would be overestimated by a factor of 11. Consequently, instead of the required minimum radius of 141 μm for a cooling rate of 15°C/My from a peak temperature of 725°C that we calculate above, the use of “uncorrected” Cygan and Lasaga data would yield a minimum garnet radius of 1,500 μm (1.5 mm). This result appears to agree with the calculations presented by Spear (1991, 1995), showing that the numerical method of Spear and the analytical method of Ganguly and Tirone (1999) are mutually compatible. However, the larger garnet radius is not an acceptable result because the diffusion data have not been adjusted to account for the difference in pressure and oxygen fugacity conditions between natural

assemblages and the experimental studies of Cygan and Lasaga (1985).

Our strategy of using core compositions of garnets with radii greater than 350 μm ensures that these compositions are not reset even during very slow initial cooling, at about 2.5°C/My. To evaluate whether the core composition could have been reset during hypothetical initial isothermal decompression, we use the solution to the diffusion equation for a spherical crystal with a fixed boundary composition (Crank 1975). It is found that the core composition is affected when $Dt/a^2 \geq 0.04$. Using this value, the inter-diffusion coefficient ‘ D ’ described in a previous paragraph, and a garnet radius of 350 μm, we find that resetting of the core compositions of the garnets we use for thermobarometry would require at least 4.9 My of isothermal decompression. Initial isothermal decompression requires initial very rapid exhumation so that the rock loses almost no heat early in the exhumation process. For example, Ganguly et al. (2000) show that initial isothermal

exhumation of granulite facies Greater Himalayan rocks in Sikkim through a distance of about 25 km required an exhumation rate of approximately 15 km/My. Even if our samples experienced some period of initial isothermal decompression, it is highly unlikely that similarly rapid exhumation rates persisted for the 4.9 My required to reset the garnet core compositions in our samples because this scenario would necessitate about 74 km of quick exhumation, thus requiring rapid exhumation from the mantle into the upper crust. There is no evidence for such deep burial or prolonged rapid exhumation of these Greater Himalayan rocks. These arguments strongly suggest that our pressure and temperature estimates are robust for initial isothermal decompression, as well as for other retrograde pressure–temperature paths, except for the two samples with garnets with radii smaller than 350 μm .

Estimates of peak metamorphic conditions

Lesser Himalayan rocks

Only one prograde metamorphism to the garnet zone or higher grades and one retrograde metamorphism are preserved in the Lesser Himalayan rocks that we studied in the Modi Khola valley. Rocks between the Ramgarh and Main Central thrusts experienced peak temperatures of about 580°C and pressures at that temperature of approximately 9 kbar (Fig. 8; Table 2). The exception is sample 502084, which records a temperature of only 500°C and does not contain biotite, unlike the other Lesser Himalayan semi-pelitic samples. This sample is located in the proximal hanging wall of the Ghandruk fault, which dropped sample 502084 from a structurally higher position relative to footwall samples. Our temperature estimates consistently are 30–60°C higher than those of Beyssac et al. (2004) from the Modi Khola area (their samples G10, G7, G9, and M9913). This difference lies within the minimum 75°C absolute uncertainty of estimates from the different thermometers used in the two studies.

There is little change in peak temperature across the Romi fault, probably because it accommodated only minor dip-slip. The Romi fault places the Eocene–Oligocene foreland basin unit in the hanging wall against the Gondwanan unit in the footwall, cutting out only part of the foreland basin unit and/or the top of the Gondwanan unit. This small stratigraphic separation suggests minor dip-slip displacement. Note that our interpretation of minor dip-slip on the Romi fault is different than the interpretation by Martin et al. (2005) because our new mapping allows us to recognize the Gondwanan Unit beneath the Romi fault, and carbonates of the upper Nawakot Unit depositionally below

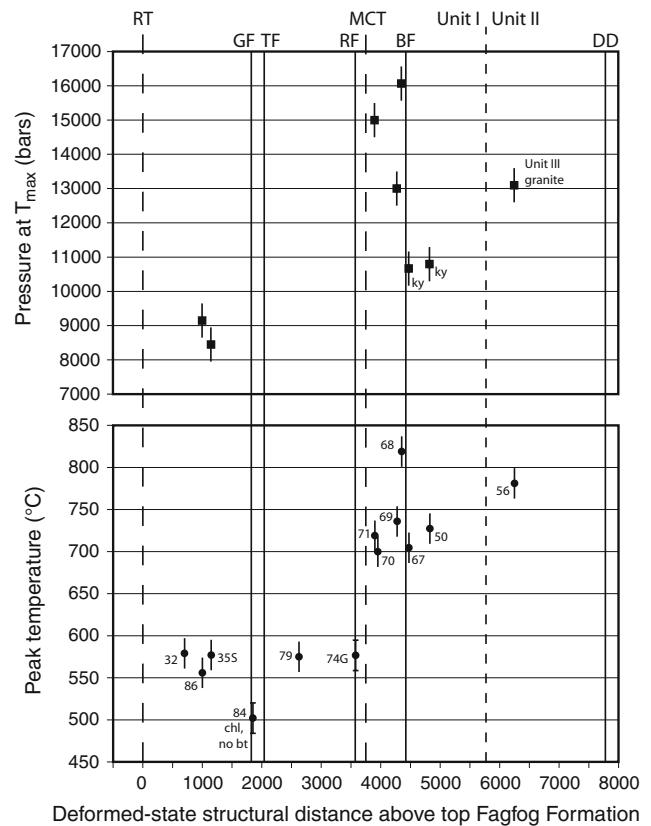


Fig. 8 Plots of estimated maximum temperatures and estimated pressures at peak temperature versus deformed state structural distance above the top of the southern exposure of the Fagfog Formation. Pressures and temperatures are approximately the same in each fault- or shear zone-bounded package of rocks, but change dramatically across some faults and ductile shear zones (fault abbreviations as in Fig. 2). All temperatures were estimated using the garnet–biotite exchange thermometer except for samples 502032, 502084, and 502079, for which the garnet–ilmenite exchange thermometer was employed. All pressures were estimated using the GMBP barometer. The locations of all known structures are shown on the plots, as are sample numbers without the “5020” prefix. Mineral abbreviations as in Fig. 5 except: *chl* chlorite. We can distinguish pressure and temperature differences between samples greater than 1 kbar and 35°C. We use *error bars* of half of these values for each data point to show graphically that we can discriminate between the estimates if the *error bars* do not overlap

the Gondwanan Unit, rather than the Kuncha Formation as previously interpreted.

Greater Himalayan rocks

As in Lesser Himalayan rocks, only one prograde metamorphism to the garnet zone or higher grades and one retrograde metamorphism are preserved by the major minerals in the Greater Himalayan rocks in the Modi Khola valley. Exposed Greater Himalayan rocks are higher grade than exposed Lesser Himalayan rocks. Rocks exposed between the MCT and the inferred Bhanuwa fault are

particularly high grade. These rocks mostly record peak temperatures of approximately 720°C and corresponding pressures of about 15 kbar. However, sample 502068, located in the proximal footwall of the Bhanuwa fault, yields a peak estimate of about 16 kbar at 820°C, 80°C hotter and 3 kbar greater than the estimate for neighboring footwall sample 502069. Sample 502068 was collected only 75 m above sample 502069, making a true pressure difference of 3 kbar untenable. If the actual peak temperature experienced by sample 502068 were 90°C hotter than the peak temperature experienced by sample 502069, a temperature gradient of 120°C/100 m, or 1,200°C/km, would be implied. This temperature gradient is unrealistic in a setting with no magmatic rocks, so the temperature estimate for sample 502068 may be too high, possibly as a result of strong metasomatism in the proximal footwall of the Bhanuwa fault. There are many mechanisms by which alteration by aqueous fluid could affect the garnet–biotite peak temperature estimate. For example, if garnet and biotite were oxidized during metasomatism, temperatures estimated using the assumption of Fe oxidation state for average pelites (Holdaway et al. 1997) would be too high. Alternatively, the pressure and temperature estimate for sample 502068 may be closer to actual peak conditions, and estimates for samples between 502068 and the MCT may be too low due to retrograde modification of mineral compositions.

Unit I rocks exposed in the hanging wall of the inferred Bhanuwa fault record peak temperatures of approximately 720°C and corresponding pressures of about 11 kbar. Hanging wall samples 502067 and 502050 contain kyanite, and the estimated pressures and temperatures are within the kyanite stability field. GASP pressure estimates are similar to the GMBP estimates. The peak temperature estimates for the Bhanuwa fault hanging wall and footwall samples are similar, within the relative uncertainty of our temperature estimates. The pressures in the hanging wall, however, are about 4 kbar lower than the pressures in the footwall, which equates to a depth difference of about 15 km. This pressure difference lies far outside the relative uncertainty of our estimates.

Unit III sample 502056 records a peak temperature of about 780°C and a pressure at that temperature of approximately 13 kbar. This temperature is 50°C hotter than the peak temperature experienced by the closest Unit I sample, 502050, and the pressure is more than 2 kbar higher, even though sample 502056 is structurally higher than sample 502050. This difference in temperature and pressure lies well outside the relative uncertainties of our estimates. The section of rocks between these samples cannot be overturned and intact because the pressure gradient would be about 0.7 km/kbar, much less than the expected lithostatic gradient of 3.8 km/kbar. A north-

dipping thrust-sense ductile shear zone or fault between samples 502050 and 502056 is the simplest explanation for the thermobarometric and structural data. The most promising candidate location for a fault or shear zone in this region is the boundary between Units I and II, although we do not have other evidence that the fault lies at this boundary.

Bhanuwa fault

Existence

Three lines of evidence suggest the presence of a fault between Greater Himalayan samples 502068 and 502067. First, a 4 kbar pressure difference (equivalent to about 15 km) exists between Unit I rocks from the south side of the fault (samples 502071, 502069, and 502068) and rocks from the north side (samples 502067, 502050), although the closest samples (502068 and 502067) currently are separated by only 125 m of structural distance. Second, Unit I strata on the south side of the fault cooled more quickly than rocks on the north side, as indicated by the dramatically shorter retrograde diffusion profiles in garnets from the south side compared to the north side (compare Fig. 6c to b). And third, Unit I deposits on the north side of the fault contain kyanite, but strata on the south side of the fault do not contain an aluminosilicate phase. This mineralogical difference may result from a difference in bulk chemistry, suggesting that the fault may juxtapose chemically-different rocks.

It is unknown whether the Bhanuwa fault accommodated motion in the brittle or ductile regime, or both. If the structure mostly accommodated ductile deformation then it would be more properly named the Bhanuwa shear zone. For simplicity, and because the deformation mechanisms are unknown, in this paper we use the term fault, with the recognition that the structure may have accommodated some deformation ductilely.

The Bhanuwa fault has not been recognized in the field or through analysis of microstructures in thin section. Several factors probably contribute to these previous difficulties in identifying the fault. First, the topography near the fault mostly permits observation and sampling of rocks only along a single north-trending foot trail. If potentially key outcrops are covered in this single dimension there is little opportunity to make observations at exposures off the trail. Further, if much of the slip on the fault occurred in the brittle regime, intense deformation in the surrounding rocks likely would be limited to the rocks in the few meters directly adjacent to the fault. In this situation, structural identification of the fault requires observation and sampling of these key proximal outcrops. Second, vegetation

and farms do in fact cover much of the terrain near the Bhanuwa fault. Third, it is possible that later brittle or ductile deformation, or both, overprinted and obscured any structures that might have been produced by the Bhanuwa fault. Structural studies specifically targeted toward the characterization of the Bhanuwa fault will be required to support or refute its presence as suggested in this paper.

Sense of slip

We did not observe the Bhanuwa fault in the field, so we do not have direct evidence for its orientation or sense of slip. We also did not observe any structures cutting foliation in the Unit I rocks at this location. By analogy with the MCT and with the faults and ductile shear zones of the STDS, it is therefore likely that the inferred Bhanuwa fault here is oriented approximately parallel to foliation in the Greater Himalayan rocks, i.e., the Bhanuwa fault currently dips approximately 30° northeast. If this orientation is correct, then the barometric and inferred cooling rate data require that the Bhanuwa fault is a normal fault, with the hanging wall down to the north. This geometry and sense of slip is similar to the geometries of the Romi and Ghandruk faults as well as the faults that comprise the STDS.

Implications

Spatial pattern of exposed metamorphic rocks

In the Modi Khola valley, the spatial pattern of exposed metamorphic rocks mostly is controlled by thrust-sense and normal-sense faults and ductile shear zones. Each shear zone- or fault-bounded domain contains rocks that experienced similar peak metamorphic conditions (Figs. 3, 8). Thrust-sense shear zones and faults in the Modi Khola transect place higher grade rocks on lower grade rocks. This pattern results from the kinematics of thrust-sense faults and ductile shear zones, which almost always place deeper (and therefore likely higher grade) rocks on shallower rocks. Because each thrust carries higher grade rocks in its hanging wall, multiple stacked thrust sheets produce an overall spatial pattern in which rocks exposed at structurally higher levels are of higher metamorphic grade (Fig. 9). We infer the documented disruptions of this pattern, where lower grade rocks are juxtaposed against structurally lower but higher grade rocks, to result from slip on normal-sense faults or ductile shear zones.

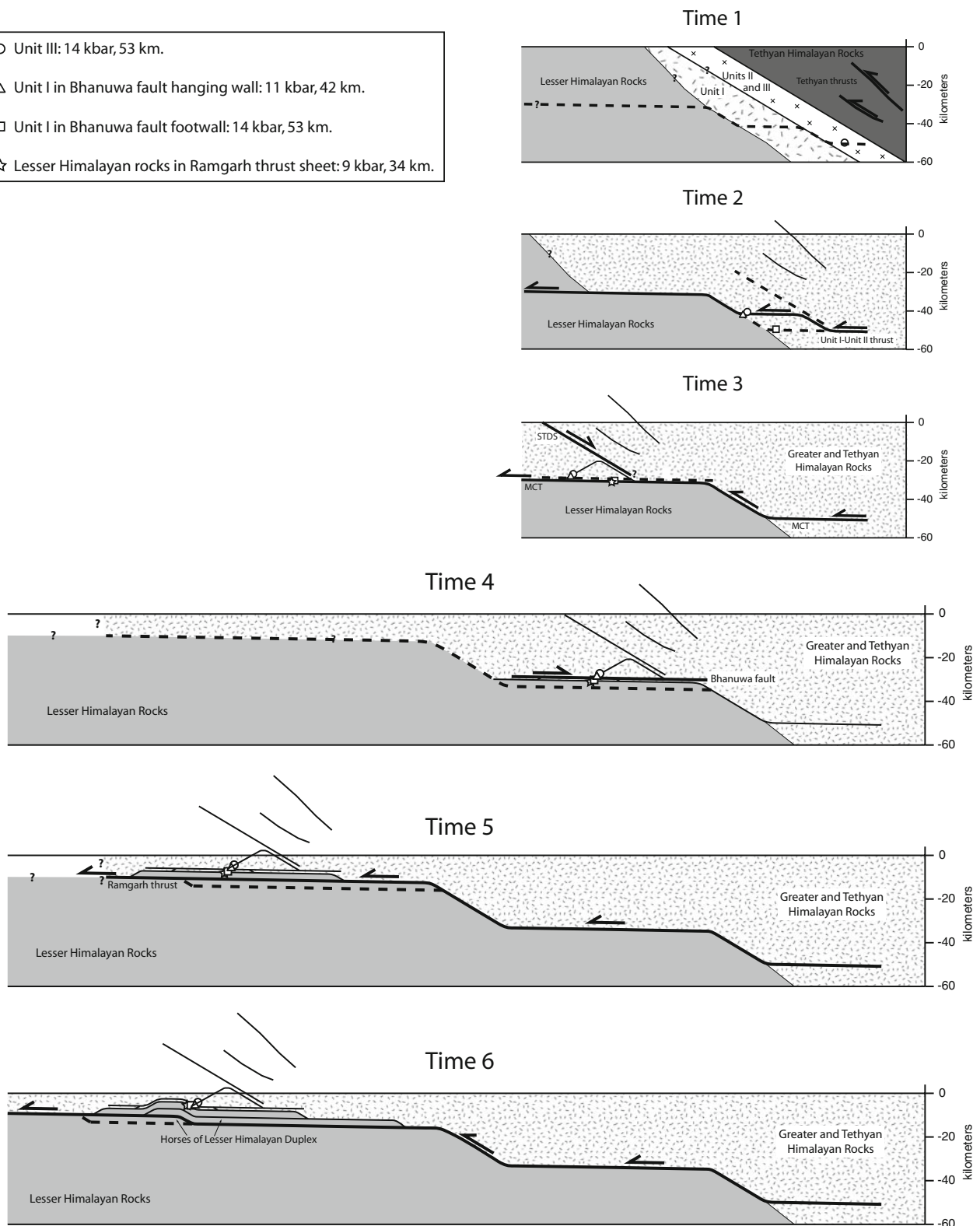
A problem with this large-scale interpretation is that Lesser Himalayan samples 502074G and 502079 record higher temperatures than structurally lower sample 502084, although no mapped thrust separates the samples. It is possible that there is a small unrecognized thrust near the

Fig. 9 Schematic (not balanced) cross-sections showing one possible reconstruction of the structural evolution of rocks in the Modi Khola valley region constrained by our new structural and thermobarometric results. The scale for each cross-section is 1:1. *Time 1* Slip on Tethyan thrusts buries Greater Himalayan rocks, including the Unit III sample shown with the *circle*. Greater and Tethyan Himalayan internal stratigraphy is omitted after time 1 for clarity. *Time 2* Displacement on a thrust juxtaposes Unit II and III rocks (*circle*) with Unit I strata (*triangle*). Motion on parts of this thrust represents initial activation of the MCT. *Time 3* Final motion on the MCT places the highest grade Unit I rocks (*square*) on Lesser Himalayan pelites (*star*). The STDS is also active at this time. In the Modi Khola region the MCT and the South Tibetan Detachment System both slipped at ca. 23 Ma (Hodges et al. 1996). *Time 4* Slip on the Bhanuwa fault juxtaposes lower pressure Unit I rocks (*triangle*) against higher pressure Unit I schists (*square*). To better illustrate the contrasting effects of normal- and thrust-sense slip, motion on the Bhanuwa fault is shown after slip on the MCT and before slip on the Ramgarh thrust. However, slip on the Bhanuwa fault may have occurred during slip on the Main Central and/or Ramgarh thrusts. *Time 5* Slip on the Ramgarh thrust places hanging wall Lesser Himalayan pelites (*star*) on footwall Lesser Himalayan rocks. *Time 6* Growth of a duplex consisting of Lesser Himalayan strata tilts the overlying rocks, and the faults contained in those rocks, to their current orientations dipping about 30° north. This model predicts pre- or syn-kinematic metamorphism, consistent with interpretations of the timing of garnet growth. Important uncertainties remain in these reconstructions including the evolution of elevation, the orientations and amounts of slip on structures, the geometric relationship between Greater and Lesser Himalayan rocks prior to Cenozoic deformation, and the orientations of Greater Himalayan strata prior to Cenozoic deformation. Given these uncertainties, this reconstruction is best viewed as a general illustration of how thrust- and normal-sense faults and shear zones in fold and thrust belts work to juxtapose rocks that experienced very different metamorphic conditions rather than a representation of the specifics of the tectonic evolution of this part of the Himalayan thrust belt

contact between the Benighat and Dhading Formations, a speculation supported by the varying width in map view of the Dhading and Benighat Formations west of the Modi Khola (Fig. 2). A thrust at this position would simply explain the higher temperatures recorded by samples 502074G and 502079 compared to sample 502084.

The broad-scale spatial pattern between the Main Frontal thrust and the STDS defined by increasing metamorphic grade of rocks exposed at higher structural levels has been observed at many other locations in the Himalaya (Mallet 1874; Macfarlane 1995; Stephenson et al. 2000; Catlos et al. 2001; Daniel et al. 2003; Dasgupta et al. 2004, 2009; Goscombe et al. 2006). The inferred Bhanuwa normal fault reverses this pattern. In the Modi Khola transect, so-called inverted metamorphism is not continuous, with gradual increases of pressure and temperature structurally upward. Instead, large jumps in pressure and temperature across major thrust-sense shear zones or faults define the so-called inverted metamorphism (Figs. 3, 8). This apparent inverted metamorphism in some parts of the transect below the Deorali detachment thus results from successive motion on discrete thrust-sense shear zones or faults, each

- Unit III: 14 kbar, 53 km.
- △ Unit I in Bhanuwa fault hanging wall: 11 kbar, 42 km.
- Unit I in Bhanuwa fault footwall: 14 kbar, 53 km.
- ☆ Lesser Himalayan rocks in Ramgarh thrust sheet: 9 kbar, 34 km.



of which is separated by kilometers. These faults and shear zones collectively stack multiple thrust sheets to produce the observed large-scale spatial pattern of exposed metamorphic rocks (Fig. 9). Because they are disrupted by large

faults and shear zones, the exposed metamorphic rocks do not represent a continuous column of crust, nor does an apparent “geotherm” calculated from these rocks represent a true geotherm that ever existed at a single point in time.

It is important for models of Himalayan tectonic evolution to note that the metamorphic rocks presently exposed in the Modi Khola valley probably did not attain peak metamorphic conditions simultaneously (cf. Stephenson et al. 2000). Instead, the age of burial, and thus prograde metamorphism, probably becomes younger toward the foreland to the south. This spatial–temporal pattern of burial and metamorphism is likely because the ages of motion on the thrust-sense faults and shear zones, which are responsible for burial of the rocks in their footwalls, probably are younger southward (DeCelles et al. 2001; Robinson et al. 2003, 2006; Kohn et al. 2004; Robinson 2008). It is even possible that the exposed metamorphic rocks did not all attain their preserved peak conditions during the same orogeny; the Cambrian–Ordovician orogeny may have produced some of the metamorphic minerals and textures we sample today (Gehrels et al. 2003, 2006a, b; Cawood et al. 2007; Martin et al. 2007), and the Cenozoic Himalayan orogeny may have produced others.

Taken together, these constraints show that motion on thrust-sense ductile shear zones and faults provides a simple explanation for most of the apparent inverted metamorphism in the rocks exposed in the Modi Khola transect and that normal-sense faults and shear zones produce significant reversals of the broad-scale spatial pattern of exposed metamorphic rocks. Significantly more complex models such as shear heating (e.g. Le Fort 1975; England et al. 1992; Harrison et al. 1997) or ductile extrusion by crustal channel flow (e.g. Jain and Manickavasagam 1993; Grujic et al. 2002; Jamieson et al. 2004; Harris 2007; Faccenda et al. 2008; Dasgupta et al. 2009) are not required to explain the peak temperature and corresponding pressure data retrieved from our samples, although our data do not rule out these models.

Location of the MCT

Searle et al. (2008) place the MCT in the Modi Khola transect a short distance below the base of the Ulleri granitic gneiss (Figs. 1, 3) based on an inferred large increase in the amount of deformation recorded in the rocks structurally above this location compared to the rocks structurally below. They support this interpretation by citing an inferred dramatic increase in metamorphic grade of the rocks structurally above this position compared to those below. In contrast, our data demonstrate that there is no large change in peak metamorphic conditions experienced by rocks throughout the area a few kilometers structurally above and below the Ulleri gneiss (Figs. 3, 8). However, there is a dramatic change in peak conditions experienced by rocks on opposite sides of our location of the MCT, which supports the location proposed by Martin et al.

(2005). These authors locate the MCT at the position of maximum strain within the shear zone, as inferred from microstructural documentation of the amount of ductile strain recorded by the rocks, and demonstrate that this position corresponds to the contact between contrasting protoliths on either side of the MCT. Searle et al. (2008) emphasize documentation of strain to locate major faults and shear zones in the region. Although this is one sound basis for finding brittle faults and ductile shear zones, other techniques are also valid. These other methods are especially important in areas of incomplete surface exposure such as the Himalaya of central Nepal. They include recognition of (1) repetition or omission of stratigraphy, (2) juxtaposition of rocks that equilibrated at dramatically different pressures and/or temperatures, and (3) a contact between terranes with contrasting depositional, metamorphic, and/or deformational histories. We use all four techniques, often in concert, to recognize faults and shear zones in the Modi Khola transect.

Conclusions

Field- and laboratory-based observations, interpretations of major element zoning profiles in garnets, and peak temperature and corresponding pressure estimates from the Modi Khola transect support the following conclusions:

1. Different samples within individual shear zone- or fault-bounded domains record approximately the same peak temperatures and corresponding pressures.
2. Structurally higher thrust sheets contain higher grade rocks. This spatial pattern results from the kinematics of thrust-sense faults and shear zones, which almost always place deeper (and therefore likely higher grade) rocks on shallower rocks. Thus in a stack of thrust sheets, the highest grade rocks are present at the highest structural levels. These geometric and kinematic considerations explain the broad pattern of exposed metamorphic rocks both near the Modi Khola and in the entire frontal half of the Himalayan thrust belt, between the Main Frontal thrust and the STDS. Significantly more complex models such as shear heating or ductile extrusion by crustal channel flow are not required to explain the metamorphic data, though the data do not rule out these models.
3. Large displacement normal faults are not restricted to the STDS at the structural top of the Greater Himalayan rocks. Another large normal fault, the Bhanuwa fault, probably is present near the base of the Greater Himalayan series. Like the faults and ductile shear zones of the STDS, the inferred Bhanuwa fault interrupts the spatial pattern of exposed metamorphic

rocks created by the thrust-sense faults and shear zones, placing shallower, lower grade rocks on deeper, higher grade rocks.

4. Only one episode of prograde metamorphism to the garnet zone or higher grades is preserved in the major mineral assemblages in Lesser and Greater Himalayan rocks. Only one episode of retrograde metamorphism overprints this prograde metamorphism. Any record in the major minerals of previous metamorphism to the garnet zone or higher grades is completely overprinted in Lesser and Greater Himalayan rocks in the Modi Khola valley. However, the presence of both Cambro-Ordovician and Cenozoic concordant monazite inclusions in Greater Himalayan garnets demonstrates that multiple thermal events affected these rocks (Gehrels et al. 2003; Martin et al. 2007).

Acknowledgments We thank Steven Kidder, Martin Herrmann, Mark Barton, Kenneth Domanik, Philip Piccoli, Sumit Chakraborty, Tank Ojha, and the staff of Himalayan Experience for their indispensable assistance. We thank Mary Leech, Donna Whitney, and four anonymous reviewers for constructive reviews and Timothy Grove for editorial handling. Supported by National Science Foundation grant EAR-0207179. A.J.M. was supported by the Geological Society of America, American Association of Petroleum Geologists, Department of Geosciences at the University of Arizona, and ExxonMobil as a donor to the Geoscience Partnership at the University of Arizona.

References

- Ahmad T, Harris N, Bickle M, Chapman H, Bunbury J, Prince C (2000) Isotopic constraints on the structural relationships between the Lesser Himalayan Series and the High Himalayan Crystalline Series, Garhwal Himalaya. *Geol Soc Am Bull* 112(3):467–477
- Amatya KM, Jnawali BM (1994) Geological map of Nepal. Department of Mines and Geology, Government of Nepal, Scale 1:1,000,000
- Arita K (1983) Origin of the inverted metamorphism of the Lower Himalayas, central Nepal. *Tectonophysics* 95(1–2):43–60
- Beyssac O, Bollinger L, Avouac J-P, Goffe B (2004) Thermal metamorphism in the Lesser Himalaya of Nepal determined from Raman spectroscopy of carbonaceous material. *Earth Planet Sci Lett* 225:233–241. doi:10.1016/j.epsl.2004.05.023
- Bollinger L, Avouac J-P, Beyssac O, Catlos EJ, Harrison TM, Grove M, Goffe B, Sapkota S (2004) Thermal structure and exhumation history of the Lesser Himalaya in central Nepal. *Tectonics* 23:TC5015. doi:10.1029/2003TC001564
- Burchfiel BC, Chen Z, Hodges KV, Liu Y, Royden LH, Deng C, Xu J (1992) The South Tibetan detachment system, Himalayan orogen: Extension contemporaneous with and parallel to shortening in a collisional mountain belt. *Geological Society of America Special Paper* 269, 41 p
- Burg JP, Chen GM (1984) Tectonics and structural zonation of southern Tibet, China. *Nature* 311(5983):219–223
- Catlos EJ, Harrison TM, Kohn MJ, Grove M, Ryerson FJ, Manning CE, Upreti BN (2001) Geochronologic and thermobarometric constraints on the evolution of the Main Central Thrust, central Nepal Himalaya: *Journal of Geophysical Research, B. Solid Earth Planets* 106:16177–16204
- Cawood PA, Johnson MRW, Nemchin AA (2007) Early Palaeozoic orogenesis along the Indian margin of Gondwana: Tectonic response to Gondwana assembly. *Earth Planet Sci Lett* 225:70–84. doi:10.1016/j.epsl.2006.12.006
- Chakraborty S, Ganguly J (1991) Compositional zoning and cation diffusion in aluminosilicate garnets. In: Ganguly J (ed) *Diffusion, atomic ordering and mass transport: advances in physical geochemistry*, vol 8. Berlin, Springer, pp 120–175
- Crank J (1975) *The mathematics of diffusion*, 2nd edn. Oxford University Press, NY, p 414
- Cygan RT, Lasaga AC (1985) Self-diffusion of magnesium in garnet at 750° to 900°C. *Am J Sci* 285:328–350
- Daniel CG, Hollister LS, Parrish RR, Grujic D (2003) Exhumation of the Main Central Thrust from lower crustal depths, eastern Bhutan Himalaya. *J Metamorph Geol* 21(4):317–334
- Dasgupta S, Ganguly J, Neogi S (2004) Inverted metamorphic sequence in the Sikkim Himalayas: crystallization history, P-T gradient and implications. *J Metamorph Geol* 22:395–412
- Dasgupta S, Chakraborty S, Neogi S (2009) Petrology of an inverted Barrovian sequence of metapelites in Sikkim Himalaya, India: constraints on the tectonics of inversion. *Am J Sci* 309:43–84. doi:10.2475/01.2009.02
- DeCelles PG, Gehrels GE, Quade J, Ojha TP (1998a) Eocene–early Miocene foreland basin development and the history of Himalayan thrusting, western and central Nepal. *Tectonics* 17(5):741–765
- DeCelles PG, Gehrels GE, Quade J, Ojha TP, Kapp PA, Upreti BN (1998b) Neogene foreland basin deposits, erosional unroofing, and the kinematic history of the Himalayan fold-thrust belt, western Nepal. *Geol Soc Am Bull* 110(1):2–21
- DeCelles PG, Gehrels GE, Quade J, La Reau B, Spurlin M (2000) Tectonic implications of U-Pb zircon ages of the Himalayan orogenic belt in Nepal. *Science* 288(5465):497–499
- DeCelles PG, Robinson DM, Quade J, Ojha TP, Garzzone CN, Copeland P, Upreti BN (2001) Stratigraphy, structure, and tectonic evolution of the Himalayan fold-thrust belt in western Nepal. *Tectonics* 20:487–509
- DeCelles PG, Gehrels GE, Najman Y, Martin AJ, Carter A, Garzanti E (2004) Detrital geochronology and geochemistry of Cretaceous–Early Miocene strata of Nepal: Implications for timing and diachroneity of initial Himalayan orogenesis. *Earth Planet Sci Lett* 227:313–330. doi:10.1016/j.epsl.2004.08.019
- Dhital MR, Thapa PB, Ando H (2002) Geology of the inner Lesser Himalaya between Kusma and Syangja in western Nepal, vol 9. *Bulletin of the Department of Geology, Tribhuvan University, Kathmandu, Nepal*. pp 1–60
- Elkins LT, Grove TL (1990) Ternary feldspar experiments and thermodynamic models. *Am Mineral* 75(5–6):544–559
- England P, Le Fort P, Molnar P, Pecher A (1992) Heat sources for Tertiary metamorphism and anatexis in the Annapurna-Manaslu region, central Nepal. *J Geophys Res B Solid Earth Planets* 97(2):2107–2128
- Faccenda M, Gerya TV, Chakraborty S (2008) Styles of post-subduction collisional orogeny: influence of convergence velocity, crustal rheology and radiogenic heat production. *Lithos* 103:257–287. doi:10.1016/j.lithos.2007.09.009
- Ferry JM, Spear FS (1978) Experimental calibration of the partitioning of Fe and Mg between biotite and garnet. *Contrib Mineral Petrol* 66(2):113–117
- Ganguly J (2002) Diffusion kinetics in minerals: Principles and applications to tectono-metamorphic processes. In: Gramaccioli CM (ed) *Energy modeling in minerals*. EMU notes in mineralogy, vol 4. pp 271–309

- Ganguly J, Saxena SK (1987) Mixtures and mineral reactions. Springer, Berlin, p 291
- Ganguly J, Tirone M (1999) Diffusion closure temperature and age of a mineral with arbitrary extent of diffusion: theoretical formulation and applications. *Earth Planet Sci Lett* 170:131–140
- Ganguly J, Cheng W, Tirone M (1996a) Thermodynamics of aluminosilicate garnet solid solution: new experimental data, an optimized model, and thermometric applications. *Contrib Mineral Petrol* 126(1–2):137–151
- Ganguly J, Chakraborty S, Sharp TG, Rumble D III (1996b) Constraint on the time scale of biotite-grade metamorphism during Acadian Orogeny from a natural garnet-garnet diffusion couple. *Am Mineral* 81(9–10):1208–1216
- Ganguly J, Cheng W, Chakraborty S (1998) Cation diffusion in aluminosilicate garnets: experimental determination in pyrope-almandine diffusion couples. *Contrib Mineral Petrol* 131:171–180
- Ganguly J, Dasgupta S, Cheng W, Neogi S (2000) Exhumation history of a section of the Sikkim Himalayas, India: records in the metamorphic mineral equilibria and compositional zoning of garnet. *Earth Planet Sci Lett* 183:471–486
- Gehrels GE, DeCelles PG, Martin A, Ojha TP, Pinhassi G, Upreti BN (2003) Initiation of the Himalayan Orogen as an early Paleozoic thin-skinned thrust belt. *GSA Today* 13(9):4–9
- Gehrels GE, DeCelles PG, Ojha TP, Upreti BN (2006a) Geologic and U–Pb geochronologic evidence for early Paleozoic tectonism in the Dadeldhura thrust sheet, far-west Nepal Himalaya. *J Asian Earth Sci* 28:385–408. doi:10.1016/j.jseas.2005.09.012
- Gehrels GE, DeCelles PG, Ojha TP, Upreti BN (2006b) Geologic and U–Th–Pb geochronologic evidence for early Paleozoic tectonism in the Kathmandu thrust sheet, central Nepal Himalaya. *Geol Soc Am Bull* 118:185–198. doi:10.1130/B25753.1
- Goscombe B, Gray D, Hand M (2006) Crustal architecture of the Himalayan metamorphic front in eastern Nepal. *Gondwana Res* 10:232–255. doi:10.1016/j.gr.2006.05.003
- Grujic D, Hollister LS, Parrish RR (2002) Himalayan metamorphic sequence as an orogenic channel: insight from Bhutan. *Earth Planet Sci Lett* 198(1–2):177–191
- Guillot S (1999) An overview of the metamorphic evolution in central Nepal. *J Asian Earth Sci* 17:713–725
- Hackler RT, Wood BJ (1989) Experimental determination of Fe and Mg exchange between garnet and olivine and estimation of Fe–Mg mixing properties in garnet. *Am Mineral* 74:994–999
- Harris N (2007) Channel flow and the Himalayan–Tibetan orogen: a critical review. *J Geol Soc Lond* 164:511–523
- Harrison TM, Ryerson FJ, Le Fort P, Yin A, Lovera OM, Catlos EJ (1997) A late Miocene–Pliocene origin for the central Himalayan inverted metamorphism. *Earth Planet Sci Lett* 146:E1–E7
- Harrison TM, Grove M, Lovera OM, Catlos EJ, D’Andrea J (1999) The origin of Himalayan anatexis and inverted metamorphism: models and constraints. *J Asian Earth Sci* 17:755–772
- Heim A, Gansser A (1939) Central Himalaya: geological observations of the Swiss expedition 1936. *Mem Swiss Soc Nat Sci* 73:245
- Hodges KV, McKenna LW (1987) Realistic propagation of uncertainties in geologic thermobarometry. *Am Mineral* 72:671–680
- Hodges KV, Parrish RR, Searle MP (1996) Tectonic evolution of the central Annapurna Range, Nepalese Himalayas. *Tectonics* 15(6):1264–1291
- Hoisch TD (1990) Empirical calibration of six geobarometers for the mineral assemblage quartz + muscovite + biotite + plagioclase + garnet. *Contrib Mineral Petrol* 104(2):225–234
- Hoisch TD (1991) Equilibria within the mineral assemblage quartz + muscovite + biotite + garnet + plagioclase, and implications for the mixing properties of octahedrally-coordinated cations in muscovite and biotite. *Contrib Mineral Petrol* 108(1–2):43–54
- Holdaway MJ, Mukhopadhyay B (1993) Geothermobarometry in pelitic schists: a rapidly evolving field. *Am Mineral* 78:681–693
- Holdaway MJ, Mukhopadhyay B, Dyar MD, Guidotti CV, Dutrow BL (1997) Garnet–biotite geothermometry revised: new Margules parameters and a natural specimen data set from Maine. *Am Mineral* 82(5–6):582–595
- Holland TJB, Powell R (1998) An internally consistent thermodynamic data set for phases of petrological interest. *J Metamorph Geol* 16:309–343
- Hooker JD (1854) *Himalayan Journals*. John Murray, London
- Jain AK, Manickavasagam RM (1993) Inverted metamorphism in the intracontinental ductile shear zone during Himalayan collision tectonics. *Geology* 21(5):407–410
- Jamieson RA, Beaumont C, Hamilton J, Fullsack P (1996) Tectonic assembly of inverted metamorphic sequences. *Geology* 24:839–842. doi:10.1130/0091-7613(1996)024<0839:TAOIMS>2.3.CO;2
- Jamieson RA, Beaumont C, Medvedev S, Nguyen MH (2004) Crustal channel flows: 2. Numerical models with implications for metamorphism in the Himalayan–Tibetan orogen. *J Geophys Res B Solid Earth* 109:B06407. doi:10.1029/2003JB002811
- Kerrick DM (1972) Experimental determination of muscovite + quartz stability with $\text{PH}_2\text{O} < \text{Ptotal}$. *Am J Sci* 272:946–958
- Kohn MJ (2008) P–T–t data from central Nepal support critical taper and repudiate large-scale channel flow of the Greater Himalayan Sequence. *Geol Soc Am Bull* 120:259–273. doi:10.1130/B26252.1
- Kohn MJ, Spear FS (1991) Error propagation for barometers: 2. Application to rocks. *Am Mineral* 76:138–147
- Kohn MJ, Spear F (2000) Retrograde net transfer reaction insurance for pressure–temperature estimates. *Geology* 28(12):1127–1130
- Kohn MJ, Wieland M, Parkinson CD, Upreti BN (2004) Miocene faulting at plate tectonic velocity in the Himalaya of central Nepal. *Earth Planet Sci Lett* 228:299–310
- Koziol AM, Newton RC (1989) Grossular activity–composition relationships in ternary garnets determined by reversed displaced-equilibrium experiments. *Contrib Mineral Petrol* 103(4):423–433
- Lave J, Avouac J-P (2001) Fluvial incision and tectonic uplift across the Himalayas of central Nepal. *J Geophys Res B Solid Earth* 106:26561–26591
- Le Breton N, Thompson AB (1988) Fluid-absent (dehydration) melting of biotite in metapelites in the early stages of crustal anatexis. *Contrib Mineral Petrol* 99:226–237
- Le Fort P (1975) Himalayas: the collided range. Present knowledge of the continental arc. *Am J Sci* 275-a:1–44
- Macfarlane AM (1995) An evaluation of the inverted metamorphic gradient at Langtang National Park, central Nepal Himalaya. *J Metamorph Geol* 13(5):595–612
- Mallet FR (1874) On the geology and mineral resources of the Darjiling district and the Western Duars. *Mem Geol Surv India* 11:1–50
- Martin AJ (2009) Sub-millimeter heterogeneity of yttrium and chromium during growth of semi-pelitic garnet: *Journal of Petrology*. doi:10.1093/petrology/egp050
- Martin AJ, DeCelles PG, Gehrels GE, Patchett PJ, Isachsen C (2005) Isotopic and structural constraints on the location of the Main Central thrust in the Annapurna Range, central Nepal Himalaya. *Geol Soc Am Bull* 117:926–944. doi:10.1130/B25646.1
- Martin AJ, Gehrels GE, DeCelles PG (2007) The tectonic significance of (U, Th)/Pb ages of monazite inclusions in garnet from the Himalaya of central Nepal. *Chem Geol* 244:1–24. doi:10.1016/j.chemgeo.2007.05.003
- Middlemiss CS (1887) Crystalline and metamorphic rocks of the Lower Himalaya, Garhwal and Kumaon. *Records of the Geological Survey of India* 20(3):134–143

- Mugnier JL, Mascle G, Faucher T (1993) Structure of the Siwaliks of western Nepal: an intracontinental accretionary prism. *International Geology Review* 35(1):1–16
- Murphy MA, Yin A (2003) Structural evolution and sequence of thrusting in the Tethyan fold-thrust belt and Indus-Yalu suture zone, Southwest Tibet. *Geol Soc Am Bull* 115(1):21–34
- Myrow PM, Hughes NC, Paulsen TS, Williams IS, Parcha SK, Thompson KR, Bowring SA, Peng SC, Ahluwalia AD (2003) Integrated tectonostratigraphic analysis of the Himalaya and implications for its tectonic reconstruction. *Earth Planet Sci Lett* 212(3–4):433–441
- Parrish RR, Hodges KV (1996) Isotopic constraints on the age and provenance of the Lesser and Greater Himalayan sequences, Nepalese Himalaya. *Geol Soc Am Bull* 108(7):904–911
- Paudel LP, Arita K (2000) Tectonic and polymetamorphic history of the Lesser Himalaya in central Nepal. *J Asian Earth Sci* 18(5):561–584
- Pearson ON (2002) Structural evolution of the central Nepal fold-thrust belt and regional tectonic and structural significance of the Ramgarh thrust. Ph.D. Dissertation, University of Arizona, p 231
- Pearson ON, DeCelles PG (2005) Structural geology and regional tectonic significance of the Ramgarh thrust, Himalayan fold-thrust belt of Nepal. *Tectonics* 24:TC4008. doi:10.1029/2003TC001617
- Pecher A (1989) The metamorphism in the central Himalaya. *J Metamorph Geol* 7(1):31–41
- Powers PM, Lillie RJ, Yeats RS (1998) Structure and shortening of the Kangra and Dehra Dun reentrants, Sub-Himalaya, India. *Geol Soc Am Bull* 110(8):1010–1027
- Pownceby MI, Wall VJ, O'Neill HSC (1991) An experimental study of the effect of Ca upon garnet–ilmenite Fe–Mn exchange equilibria. *Am Mineral* 76(9–10):1580–1588
- Quade J, Catter JML, Ojha TP, Adam J, Harrison TM (1995) Late Miocene environmental change in Nepal and the northern Indian subcontinent: stable isotopic evidence from paleosols. *Geol Soc Am Bull* 107(12):1381–1397
- Ratschbacher L, Frisch W, Liu G, Chen C (1994) Distributed deformation in southern and western Tibet during and after the India-Asia collision. *J Geophys Res* 99(B10):19917–19945
- Reddy SA, Searle MP, Massey JA (1993) Structural evolution of the High Himalayan gneiss sequence, Langtang Valley, Nepal. In: Treloar PJ, Searle MP (eds) *Himalayan tectonics*. Geological Society Special Publication. Geological Society of London, London, pp 375–389
- Robinson DM (2008) Forward modeling the kinematic sequence of the central Himalayan thrust belt, western Nepal. *Geosphere* 4:785–801. doi:10.1130/GES00163.1
- Robinson DM, DeCelles PG, Patchett PJ, Garzzone CN (2001) The kinematic evolution of the Nepalese Himalaya interpreted from Nd isotopes. *Earth Planet Sci Lett* 192(4):507–521
- Robinson DM, DeCelles PG, Garzzone CN, Pearson ON, Harrison TM, Catlos EJ (2003) Kinematic model for the Main Central Thrust in Nepal. *Geology* 31(4):359–362
- Robinson DM, DeCelles PG, Copeland P (2006) Tectonic evolution of the Himalayan thrust belt in western Nepal: Implications for channel flow models. *Geol Soc Am Bull* 118:865–885. doi:10.1130/B25911.1
- Sakai H (1983) Geology of the Tansen Group of the Lesser Himalaya in Nepal. *Memoirs of the Faculty of Science, Kyushu University, Series D, Geology* 25(1):27–74
- Searle MP, Godin L (2003) The South Tibetan detachment and the Manaslu Leucogranite: a structural reinterpretation and restoration of the Annapurna-Manaslu Himalaya, Nepal. *J Geol* 111(5):505–523
- Searle MP, Simpson RL, Law RD, Parrish RR, Waters DJ (2003) The structural geometry, metamorphic and magmatic evolution of the Everest Massif, High Himalaya of Nepal-South Tibet. *J Geol Soc London* 160(3):345–366
- Searle MP, Law RD, Godin L, Larson K, Streule MJ, Cottle JM, Jessup MJ (2008) Defining the Himalayan Main Central thrust in Nepal. *J Geol Soc London* 165:523–534. doi:10.1144/0016-76492007-081
- Sorkhabi RB, Macfarlane A (1999) Himalaya and Tibet: mountain roots to mountain tops. In: Macfarlane A, Sorkhabi RB, Quade J (eds) *Himalaya and Tibet: mountain roots to mountain tops: special Paper—Geological Society of America*. United States, Geological Society of America (GSA), Boulder, CO, pp 1–7
- Spear FS (1991) On the interpretation of peak metamorphic temperatures in light of garnet diffusion during cooling. *J Metamorph Geol* 9:379–388
- Spear FS (1995) *Metamorphic phase equilibria and pressure–temperature–time paths*. Mineralogical Society of America Monograph, Washington, DC, p 799
- Srivastava P, Mitra G (1994) Thrust geometries and deep structure of the outer and lesser Himalaya, Kumaon and Garhwal (India): implications for evolution of the Himalayan fold-and-thrust belt. *Tectonics* 13(1):89–109
- Stephenson BJ, Waters DJ, Searle MP (2000) Inverted metamorphism and the Main Central Thrust: field relations and thermobarometric constraints from the Kishtwar Window, NW Indian Himalaya. *J Metamorph Geol* 18(5):571–590
- Todd CS (1998) Limits on the precision of geobarometry at low grossular and anorthite content. *Am Mineral* 83:1161–1167
- Upreti BN (1996) Stratigraphy of the western Nepal Lesser Himalaya, a synthesis. *J Nepal Geol Soc* 13:11–28
- Vannay JC, Hodges KV (1996) Tectonometamorphic evolution of the Himalayan metamorphic core between the Annapurna and Dhaulagiri, central Nepal. *J Metamorph Geol* 14(5):635–656
- Webb AAG, Yin A, Harrison TM, Celerier J, Burgess WP (2007) The leading edge of the Greater Himalayan Crystalline complex revealed in the NW Indian Himalaya: Implications for the evolution of the Himalayan orogen. *Geology* 35:955–958. doi:10.1130/G23931A.1
- Yin A (2006) Cenozoic tectonic evolution of the Himalayan orogen as constrained by along-strike variation of structural geometry, exhumation history, and foreland sedimentation. *Earth Sci Rev* 76:1–131. doi:10.1016/j.earscirev.2005.05.004
- Zhu C, Sverjensky DA (1992) F-Cl-OH partitioning between biotite and apatite. *Geochim Cosmochim Acta* 56(9):3435–3467